EXHIBIT 23

Therapeutic Strategies for Familial Hypercholesterolemia Based on Somatic Gene Transfer

James M. Wilson, MD, PhD, and Mariann Grossman, BS

Inherited dyslipidemias are important risk factors for the premature development of coronary artery disease. One example is an inherited deficiency of low density lipoprotein (LDL) receptors that leads to the syndrome familial hypercholesterolemia (FH). We have used FH as a model for developing new approaches for treating this group of disorders by somatic gene therapy. Experiments in animal models that led to the initiation of a clinical trial of homozygous FH will be presented in this review.

(Am J Cardiol 1993;72:59D–63D)

From the Institute for Human Gene Therapy and the Wistar Institute, University of Pennsylvania School of Medicine, Philadelphia, Pennsylvania 19104.

Address for reprints: James M. Wilson, M.D., Ph.D, The Institute for Human Gene Therapy, University of Pennsylvania, Rm. 204, The Wistar Institute, 36th and Spruce Streets, Philadelphia, Pennsylvania 19104-4268.

Familial hypercholesterolemia (FH) is an autosomal dominant disorder caused by defects in the gene encoding the low density lipoprotein (LDL) receptor.[1] The basic pathophysiology of this disease is quite simple. the gene defect leads to diminished systemic levels of LDL receptor activity, resulting in diminished capacity to catabolize LDL and its precursor intermediate density lipoprotein. The 50% reduction in LDL receptor activity found in FH heterozygotes is associated with moderate elevations in serum LDL and premature coronary artery disease. The severe deficiency of LDL receptor activity found in homozygotes (i.e., 0–20% of normal) leads to massive accumulations of LDL in childhood.

Management of hypercholesterolemia associated with the heterozygous state is difficult, often requiring a strict dietary program in combination with a multiple drug regimen.[2] Unfortunately, FH homozygotes are essentially refractory to dietary or pharmacologic therapy. A variety of approaches has been explored to partially control hypercholesterolemia in homozygous FH, including plasmapheresis, LDL apheresis, portacaval shunt, and ileal bypass.[2] The most impressive results have been obtained through orthotopic liver transplantation with an organ derived from an LDL-receptor expressing donor.[3,4]

The success of liver transplantation in the management of hypercholesterolemia in FH homozygotes illustrates an important principle. Selective reconstitution of LDL receptor expression in liver is sufficient to achieve a significant improvement in the dyslipidemia associated with this disease. This suggests that a similar result could be achieved by reconstituting LDL receptor expression in the patient's own hepatocytes through somatic gene transfer. In this review we describe experimental and clinical models of liver-directed gene therapy for the treatment of homozygous FH.

Gene therapy holds tremendous promise for the treatment of inherited diseases. Much of the experi-

mental development of gene therapies has focused on the hematopoietic system.[5] In fact, the first clinical protocol involved the transfer of an adenosine deaminase gene into lymphocytes of a patient with severe combined immunodeficiency (M. Blaese, unpublished data). We believe the homozygous form of FH is also a good model for the development and early application of gene therapies. The key advantages of this disease include: (1) the normal gene has been isolated[6]; (2) organ transplantation has indicated that genetic reconstitution of a single organ, the liver, is sufficient for efficacy[3,4]; (3) biochemical efficacy of the therapy is easily monitored by serial measurements of serum lipids: (4) genotype:phenotype correlations in FH homozygotes suggest that partial genetic reconstitution will be therapeutic[7,8]; (5) the severe form of the disease is refractory to conventional therapies and is associated with mortality in childhood[2]; and (6) an authentic rabbit model, the Watanabe heritable hyperlipidemic (WHHL) rabbit, is available.[9–11]

EX VIVO GENE THERAPY

The early paradigms of gene therapy were based on transplantation of autologous cells modified ex vivo with recombinant retroviruses. The application of this approach to liver-directed gene transfer of the LDL receptor gene for the treatment of FH is described below. A section of liver is removed and perfused with collagenase to release hepatocytes. The cells are plated in culture, exposed to an LDL receptor expressing recombinant retrovirus, harvested with trypsin, and infused into the portal circulation. This therapeutic approach was initially developed in the WHHL rabbit, an animal that has a mutation in its LDL receptor gene that renders the protein dysfunctional and leads to hypercholesterolemia, atheromas, and coronary artery disease.[9–11]

The first step toward the development of these therapies was to design methods for isolating WHHL hepatocytes and efficiently transducing functional LDL receptor genes into the cells.[12] A single exposure of LDL receptor-expressing, replication-defective retrovirus to freshly isolated newborn WHHL hepatocytes led to gene transfer into the majority of cells and reconstitution of normal levels of LDL receptor activity.

The next and more difficult step was to develop methods for transplanting LDL receptor-expressing hepatocytes into WHHL rabbits in such a way that the cells function and persist. Hepatocytes were isolated from an outbred strain of rabbits that express normal levels of LDL receptor (New Zealand White strain) and transplanted into WHHL recipients by direct injection into the portal vein or into the peritoneal cavity attached to microcarrier beads.[13] Transplantation of New Zealand White hepatocytes using either method led to a 25% decrease in total plasma cholesterol over a 3–4 day period with a gradual return to pretreatment levels after 10 days. These experiments indicate that ectopically placed hepatocytes (in liver sinusoids or in the peritoneal cavity) can function with respect to lowering cholesterol, but only in a transient manner. Wiederkehr et al[14] have demonstrated more prolonged function of transplanted New Zealand White hepatocytes in WHHL rabbits when the animals were chronically immunosuppressed with cyclosporine suggesting that the deterioration in LDL receptor function may be due to immunologic responses to the allogeneic cells.

The feasibility of ex vivo gene therapy in the WHHL rabbit was demonstrated in a modification of the allogeneic experiments described above.[15] Liver was removed from a WHHL rabbit and hepatocytes were harvested and plated in primary cultures. Recombinant human LDL receptor genes were transduced into 10–20% of the cultured hepatocytes, which were harvested 4 days after the initial plating and were transplanted into an allogeneic WHHL recipient. A substantial (30–40%) but, again, transient decline in serum cholesterol was achieved after transplantation of the LDL receptor transduced hepatocytes. Molecular analysis of liver tissues demonstrated proviral DNA (approximately 1 in 100 cells) and recombinant LDL receptor transcripts (2–4% of endogenous) for a short time after transplantation. In situ hybridization analysis detected the transduced cells in a periportal distribution of the recipient liver. No significant change in serum cholesterol was noted in animals that received mock-infected hepatocytes.

We next sought to modify the protocol to achieve more prolonged, if not permanent, metabolic improvement. We hypothesized that the rapid deterioration of LDL receptor function in the allogeneic ex vivo experiments was due to rejection caused by immune responses to the allogeneic cells or to the human LDL receptor protein.

We overcame these problems in a second series of experiments in which recombinant retroviruses were produced that contained the wild-type rabbit LDL receptor gene.[16] A group of WHHL rabbits underwent partial hepatectomies and the liver tissues were used to prepare hepatocytes and

establish primary cultures. The cultured hepatocytes were exposed to the second generation virus described above, harvested, and transplanted into the portal circulation of the animals from which they were derived.

Animals transplanted with LDL receptor transduced hepatocytes demonstrated a 30–50% decrease in total serum cholesterol that persisted for the duration of the experiment (122 days). No significant change in serum cholesterol was noted in animals that received mock-transduced hepatocytes. Ribonuclease (RNase) protection assays demonstrated recombinant derived LDL receptor RNA in liver tissues harvested up to 6.5 months without apparent diminution. Transplant recipients did not develop a serologic response to wild-type rabbit LDL receptor protein, as determined by Western blot analysis.

Based on the encouraging results obtained in the WHHL rabbit, a series of experiments were performed to determine the feasibility and safety of clinical trials in humans (Table I). Techniques used in the isolation and transduction of rabbit hepatocytes were adapted for human hepatocytes. Portions of liver tissue from 5 human donors were perfused with collagenase and the released hepatocytes were plated in primary culture.[17] The viability of recovered hepatocytes ranged from 85–98% and the recovery ranged from 3–33 $\times$ 10^6 cells/g wet weight of tissue. The cells plated with high efficiency and grew to confluence over the subsequent 72 hours. A recombinant retrovirus containing the human LDL receptor gene was exposed to the hepatocytes under a variety of conditions and analyzed for gene transfer and expression. Optimal gene transfer was achieved when the cultures were incubated with the recombinant retrovirus for a 16-hour period beginning 48 hours after the initial seeding. Efficiency of gene transfer ranged from a maximum of 1 proviral copy per diploid genome to a minimum of 0.1 proviral copy per diploid genome. Analysis of the transduced populations of cells for expression of the recombinant gene revealed levels of LDL receptor RNA and protein equal to or in excess of the endogenous LDL receptor gene products.

A series of experiments were performed in baboons in order to establish the feasibility and short-term toxicity of ex vivo, liver-directed gene therapy.[18] The protocol developed in rabbits required separate surgical interventions for the liver resection and cell infusion. In preparation for human trials, the protocol was modified to require a single surgical intervention. Three baboons underwent a partial hepatectomy and their hepatocytes were isolated, cultured, and transduced with the recombinant retrovirus containing the human LDL receptor gene. Analysis of the hepatocytes indicated gene transfer into 10–20% of the cells. The hepatocytes were harvested and infused into an indwelling catheter that had been placed into the inferior mesenteric vein at the time of liver resection. Cell infusion was associated with a small but transient elevation in portal pressure in 2 animals. Portal venograms performed after cell infusion demonstrated complete patency of the portal circulation. Follow-up evaluations have ranged from 21–24 months. Clinical evaluations have been unremarkable and blood chemistry and hematology determinations have stayed within normal limits except for transient elevations in liver function tests and a transient decrease in hematocrit following the liver resection.

TABLE I Preclinical Studies for Ex Vivo Gene Therapy of Familial Hypercholesterolemia

1. Ex vivo gene therapy in WHHL rabbits to demonstrate efficacy
2. Isolation of human hepatocytes
3. Production and characterization of recombinant retrovirus expressing human LDL receptor
4. Feasibility and acute toxicity of ex vivo gene in baboons

LDL = low density lipoprotein; WHHL = Watanabe heritable hyperlipidemic.

The preclinical studies outlined in Table I have formed the basis for a clinical trial of ex vivo gene therapy in patients with homozygous FH. Essential steps in the protocol are summarized in Figure 1. The patient is taken to the operating room where the left lateral segment of the liver is resected (approximately 10–15% of the total liver) and a catheter is placed in the inferior mesenteric vein. The resected liver is perfused with collagenase to release the hepatoctyes, which are plated in culture

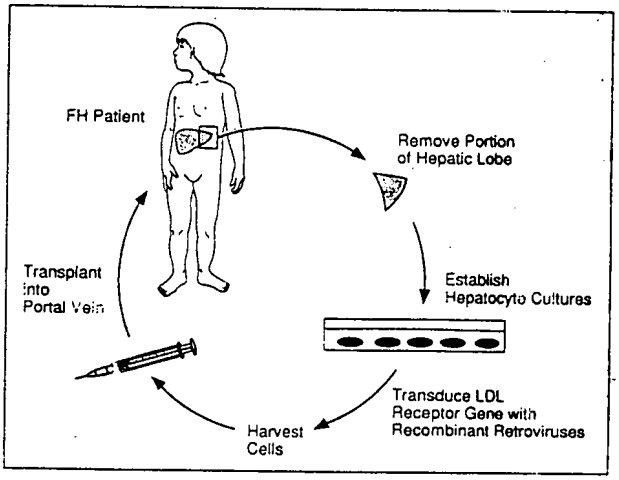

FIGURE 1. Schematic of ex vivo gene therapy for familial hypercholesterolemia (FH).

for 2 days before they are exposed to the recombinant retrovirus for a 12–16-hour period. The virus is then washed away and the cells are released with trypsin and infused into the catheter, which is easily removed several days later. The initial protocol proposes to treat 3 FH homozygotes that have developed objective coronary artery disease despite all attempts to control hypercholesterolemia. The expectation is to achieve approximately 2–10% reconstitution of LDL receptor expression in the liver. Patients most likely to realize a significant reduction of cholesterol are those who are receptor negative. The length of time that a therapeutic effect will be realized is unknown. However, experiments in the WHHL rabbits indicated that transgene expression is stable without obvious change for at least 6.5 months. It is important to note that gene therapy in this protocol is an adjunct to other therapies such as pharmacologic approaches and plasmapheresis and does not preclude subsequent orthotopic liver transplantation. The first patient was treated June 5, 1992, without complications.

IN VIVO GENE THERAPY

It is our hope that ex vivo gene therapy will benefit a subset of severely affected FH homozygotes. However, the broader application of this type of therapy is limited for several reasons. There will always be unavoidable risks associated with the surgical aspects of the protocol. More importantly, the efficiency of genetic reconstitution is directly related to efficacy and will always be limited by the number of hepatocytes that can be harvested, genetically modified, and reinfused. This is limited to 2–5% of the total cells in a liver using the existing protocols. Considering these limitations, it is unlikely that this approach will be useful in treating the larger population of FH heterozygotes. We have begun to develop more effective and clinically practical approaches based on the direct delivery of LDL receptor genes to liver through the parenteral administration of targetable gene transfer substrates.

The approach that is most promising is based on the construction of a synthetic complex of DNA and protein that is specifically recognized by hepatocytes. A glycoprotein ligand for the liver-specific asialoglycoprotein receptor is covalently linked to a polymer of lysine.[19] This protein:protein conjugate is bound to plasmid DNA containing the therapeutic gene through nondestructive electrostatic interactions between the DNA and poly-L-lysine. Early experiments with reporter genes in rats indicated that direct infusion of the DNA–protein complex was associated with[20]: (1) clearance of the complex from the blood within minutes of injection; (2) uptake predominantly by receptor mediated processes in hepatocytes; and (3) expression of the recombinant gene in liver for 12–72 hours following infusion.

We have used this approach to treat hypercholesterolemia in the WHHL rabbit.[21] A vector was constructed in which the human LDL receptor gene is expressed from liver-specific transcriptional elements. Complexes formed with this vector were infused into peripheral veins of WHHL rabbits. Molecular analysis of liver tissues indicated targeting of the transgene to a large proportion of hepatocytes within minutes of infusion. Hepatocyte-associated plasmid DNA rapidly degraded to undetectable levels within 48 hours of the infusion. Recombinant LDL receptor transcripts were detected 4 hours after administration of the complex, reached a maximum at 24 hours (approximately 4% of the endogenous levels), and diminished to undetectable levels by 72 hours. Injection of the complex led to an immediate but transient decrease in total serum cholesterol by 153 ± 53 mg/dL, which was approximately 30% of the pretreatment values. Serum cholesterol returned to pretreatment values by day 6.

Despite the very encouraging results obtained in the initial WHHL studies described above, the treatment must be improved in several ways before it can be considered for clinical applications in humans. For this type of therapy to be practical, it will be necessary to prolong the expression of the transgene far beyond 6 days. One strategy for accomplishing this is to perform a partial hepatectomy immediately after infusion of the complex. Experiments in rats have demonstrated transgene expression for up to 4 months following these procedures.[20] Interestingly, the transgene appears to persist as a stabilized episome in hepatocytes of the transplant recipients.[22] An alternative approach for achieving prolonged transgene expression is to administer a drug that stimulates hepatocyte division at the time the complex is infused. Another important advance will be to increase the efficiency by which the transgene is expressed. The current levels of expression achieved in the WHHL rabbits are insufficient to improve hypercholesterolemia in FH heterozygotes. The one factor that most significantly interferes with functional gene expression relates to the normal intracellular processing of the asialoglycoprotein receptor ligand. Glycoproteins that bind to this receptor are endocytosed and primarily trafficked to endosomes

Increase your Analytical

WITH–

the top-of-the-line research HP 5985B GC/MS: Its price/performance capability is unprecedented

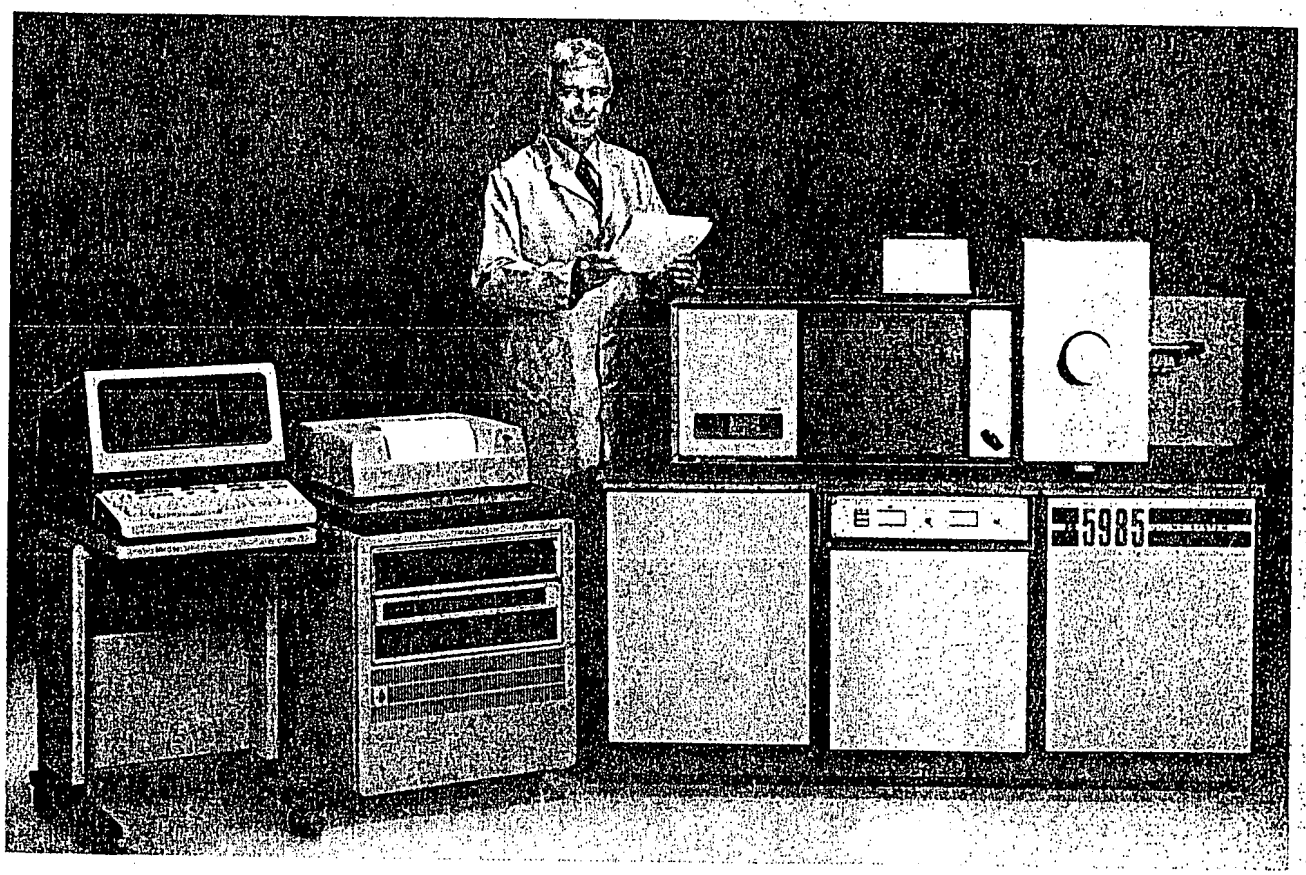

Its powerful built-in data system scans, processes, and analyzes MS data quickly. Powerful programs such as batch processing, simultaneous acquisition/reduction, automatic tuning and huge libraries provide outstanding flexibility in measurement and data handling.

The 5985B dual, proven CI/EI source provides for changes in both conductance and configuration when switching from one ionization mode to another. Switching takes only seconds.

Optional LC/MS, negative ion, and automatic sample handling operations provide greatly expanded capabilities for biomedical, pollutant, forensic and general organic analyses. Other advanced features include an efficient hyperbolic quadrupole mass filter, all-digital electronics, and a powerful HP 21 MX E-Series computer which operates with a large number of peripheral output and storage devices. For faster vacuum cycle time, optional turbo-molecular pumps are available. Mass range is 10 to 1000 amu and sensitivity is to picogram levels, essential for the analyses of pesticide, environmental, drug, and biological samples.

Call or write for details on how the powerful HP 5985B GC/MS can contribute to your lab's productivity.

Circle Reader Service No. 130

al Productivity!

HP GAS CHROMATOGRAPHS

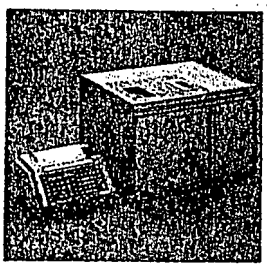

Chemical performance, versatility and computational power are maximized in the new 5880A. The microprocessor based 5840 offers unmatched price/performance ratio; the 5700 series—rugged simplicity. All are available with automatic injection, capillary inlets and assorted accessories. Circle Reader Service No. 131.

HP LIQUID CHROMATOGRAPHS

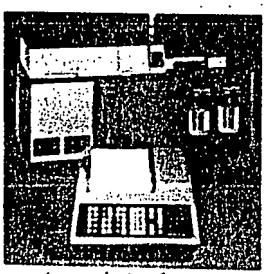

Our microcomputer-controlled HPLC's provide full control of separation parameters and accurate quantitative results for routine experimental analyses. You can customize our HPLC's with the automatic sampler, fraction collector, variable and fixed wave length detectors, bidirectional data system interface and many more features. Circle Reader Service No. 132.

THE NEW HP UV/VIS SPECTROPHOTOMETER

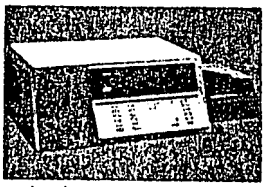

This powerful micro-computer-controlled HP 8450A provides full spectrum and multi-component analysis in seconds. It measures and displays the full spectrum on a CRT in one second—greatly reducing the time per analysis. Sample handling is simplified and sample preparation is minimized with this extremely productive unit. Circle Reader Service No. 133.

HP LABORATORY AUTOMATION SYSTEMS

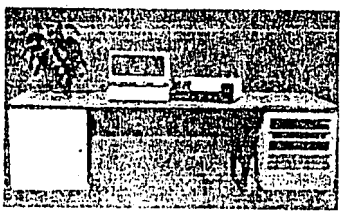

Our turnkey systems provide chromatographic software with sophisticated data reduction. They perform record keeping tasks and automate analytical procedures to increase sample throughput. Flexibility and upgradability allow these systems to grow with your needs. Circle Reader Service No. 134.

43006

HP GRAPHIC INTEGRATORS

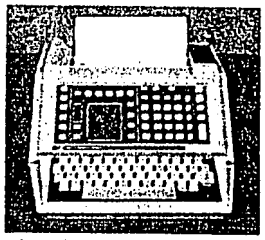

The microprocessor based HP 3388A Chromatography Automation System provides standard chromatographic calculations, BASIC programming, long-term data storage, and simultaneous dual-channel integration and control. Analyses can be completely automated and results customized to your needs. Circle Reader Service No. 135.

HP COLUMNS AND ACCESSORIES

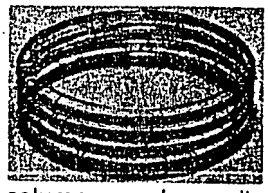

The new, flexible, fused silica column offers inertness, thermal stability and high efficiency for high resolution gas chromatography. Many analyses that were difficult or impossible on conventional columns can be easily handled with this new column. Our complete stock of columns and accessories helps you obtain the best separation. Circle Reader Service No. 136.

HP CUSTOMER SERVICE

Our worldwide network of factory-trained service specialists provides efficient maintenance and repair service. To decrease the downtime we provide parts, test equipment and service kits for HP instruments. Circle Reader Service No. 137.

HP CUSTOMER TRAINING

In-depth training courses are offered for our analytical instruments. Operator courses contribute to the better utilization of your instruments. Application courses provide basic information in specific areas. Circle Reader Service No. 138.

FOR MORE INFORMATION

about the many ways Hewlett-Packard can increase your analytical productivity, write to: Hewlett-Packard, 1507 Page Mill Road, Palo Alto, CA 94304. Or call the HP regional office nearest you: East (301) 258-2000, West (714) 870-1000, Midwest (312) 255-9800, South (404) 955-1500. Canada (416) 678-9430.

HEWLETT PACKARD

Here is a New HPLC Detector that's good for measuring...

ALMOST NOTHING

FLUOROMONITOR III
10^{-18} mole sensitivity in Liquid Chromatography

The new LDC FluoroMonitor III fluoresence detector offers the ultimate in HPLC sensitivity. Minimum concentration levels as low as 10^{-18} mole are now possible by virtue of such design features as:

- 30 ul high purity silica flowcell
- excitation wavelengths as low as 214 nm
- unique split beam optical system

The FluoroMonitor III is a single compact module which can be interfaced to any liquid chromatograph. All electronics are solid state. The entire optical system can be removed for easy servicing.

LDC Liquid Chromatographs

Laboratory Data Control Div. of Milton Roy Company
P.O. Box 10235, Riviera Beach, Flor[illegible] 33404 Tel: (305) 844-52[illegible]

CIRCLE 128 ON READER SERVICE CARD

	Grade 0	Grade 1	Grade 2	Grade 3	Grade 4
Cutaneous	No change	Erythema	Dry desquamation, vesiculation, pruritus	Moist desquamation, ulceration	Exfoliative dermatitis; necrosis requiring surgical intervention
Hair	No change	Minimal hair loss	Moderate, patchy alopecia	Complete alopecia, but reversible,	Non-reversible alopecia
Infection (specify site)	None	Minor infection	Moderate infection	Major infection	Major infection with hypotension
Cardiac Rhythm	No change	Sinus tachycardia >110 at rest	Unifocal PVC, atrial arrhythmia	Multifocal PVC	Ventricular tachycardia
Cardiac Function	No change	Asymptomatic, but abnormal cardiac sign	Transient symptomatic dysfunction; no therapy required	Symptomatic dysfunction responsive to therapy	Symptomatic dysfunction non-responsive to therapy
Pericarditis	No change	Asymptomatic effusion	Symptomatic; no tap required	Tamponade; tap required	Tamponade; surgery required
Neurotoxicity					
State of consciousness	Alert	Transient lethargy	Somnolence <50% of waking hours	Somnolence >50% of waking hours	Coma
Peripheral	None	Paresthesias and/or decreased tendon reflexes	Severe paresthesias and/or mild weakness	Intolerable paresthesias and/or marked motor loss	Paralysis
Constipation[c]	None	Mild	Moderate	Abdominal distension	Distention and vomiting
Pain[d]	None	Mild	Moderate	Severe	Intractable

[a] Any degree of methemoglobinemia associated with what is felt to be clinically significant pulmonary symptoms or cyanosis will be considered at least grade 3.
[b] Upper limit of normal value of population under study.
[c] This does not include constipation resultant from narcotics.
[d] Only treatment-related pain is considered, *not* disease-related pain. The use of narcotics may be helpful in grading pain, depending upon the tolerance level of the patient.

Edward S. Yeung
Michael J. Sepaniak
Ames Laboratory and Department of Chemistry
Iowa State University
Ames, Iowa 50011

LASER FLUOROMETRIC DETECTION IN LIQUID CHROMATOGRAPHY

In a recent Science Update feature article (*1*) it was noted that " . . . there's little doubt that spectroscopy, in its numerous forms and especially in conjunction with chromatographic separation methods, still plays the leading role in analytical chemistry." Because lasers have opened up new frontiers in spectroscopy since their introduction, it is natural that the use of lasers in chromatographic detection schemes has generated much interest. In this article, the technique of laser fluorometry as applied to detection in high-performance liquid chromatography (HPLC) is discussed, with special emphasis on instrument design, characteristics and potentials, and some selected applications.

The determination of trace organic compounds in complex samples is of concern in clinical (*2*), environmental (*3*), and energy-related (*4*) areas. Recent advances in gas chromatography, particularly in combination with mass spectrometry, have solved most of the problems associated with the determination of the volatile organic species. Except for isolated cases, it is unlikely that the laser can drastically improve upon these analytical schemes. The situation is, however, different for the nonvolatile organics, due to the generally poorer resolution of HPLC and difficulties in the corresponding interface to a mass spectrometer. It is clear that sensitive and selective detectors are needed to compensate for the lack of chromatographic resolution and to aid in the identification of these species. It is further desirable for such detectors to be nondestructive so that several of them can be used in series to maximize the amount of information in the analysis. These are areas where laser spectroscopic methods can make an impact. It is beyond the scope of the present article to discuss all of the laser-based detectors for HPLC (*5*); thus, only laser fluorometry, the most developed detection scheme, is presented. So, what are the real advantages of using laser fluorometry as compared to the many fine commercial fluorometric detectors for HPLC? Or is the laser simply an expensive light bulb?

Characteristics of Laser Fluorometry

Power. The publicity surrounding laser fusion and possible laser weapons has made high power synonymous with lasers. Photon flux naturally is important to sensitivity in fluorometric methods since the signal level is directly proportional to it up to the point of saturation. One can compare the photon fluxes for lasers vs. standard light sources for commercial fluorometric HPLC detectors. Assuming f/1.0 imaging optics, a 100-W mercury arc at 254 nm, a 50-W deuterium lamp at 230 nm, and a 100-W quartz halogen tungsten lamp at 600 nm provide 4.5 mW, 0.9 mW, and 17.3 mW of radiation respectively. For the two con-

0003-2700/80/A351-1465$01.00/0

tinuum sources, a useful bandwidth of 10 nm (based on typical excitation bandwidths) is assumed. These represent operation at the ideal operating wavelengths for the individual lamps, and the flux levels will suffer if other spectral regions matching the absorption of the species involved are used. For example, the tungsten lamp is practically useless for exciting ultraviolet fluorescence. In contrast, commercial lasers providing the order of 10 W in the visible wavelength region (argon ion laser) and in the ultraviolet wavelength region (KrF laser) are available. More importantly, the spatial coherence of the laser allows all of the radiation to be efficiently utilized in a small detection volume, and the monochromaticity of the laser allows rejection of scattered radiation without sacrificing power.

The increase in photon flux does not automatically improve the limits of detection in fluorometry. Ultimately, noise, which primarily consists of stray radiation, limits the detectability, and it becomes an important factor in the proper design of the instrument. Of special interest is the fact that large photon fluxes can induce other optical effects, such as the simultaneous absorption of two photons, so that new fluorometric schemes can be utilized in HPLC detection.

Collimation. The development of higher chromatographic resolution in HPLC is inevitably associated with the reduction of detector volume. Lasers, because of the properties of a Gaussian beam, can be readily adapted to minimize the detector volume. It is known that the useful range of collimation, z, is related to the beam radius, w, and the wavelength, λ, such that

$$z = \pi w^2/\lambda \qquad (1)$$

Since the fluorescence intensity is proportional to the incident intensity and the interaction length in the limit of low absorption, one must preserve a finite pathlength, say 1 cm. For 300-nm light, the detector volume is then about 30 nL. This is certainly a substantial improvement over the 5 μL volume offered by the best commercial fluorometric detector, particularly if one has enough excitation intensity to sacrifice part of the beam by further reducing the diameter of the detector. Another important but often neglected aspect of collimation is the possibility of reducing stray light. A well-defined beam is far easier to manipulate optically, both in the source optics and in the collection optics in fluorometry.

Monochromaticity. Molecular absorption spectra in the condensed phases are generally much broader than typical laser outputs so that the monochromatic laser output does not improve selectivity. However, monochromaticity can be advantageously used to reject stray light. Figure 1 shows the typical spectral distribution of scattered light from Rayleigh and Raman processes, which in HPLC come from the solvent and optical components, including the cell windows. Conventional fluorometric detectors have an excitation bandwidth of the order of 10 nm, so that the Rayleigh and Raman "bands" are of comparable widths. The use of monochromatic excitation reduces these bands to 1 nm, the inherent width of typical Raman lines. The "windows" available for fluorescence detection are thus larger and easier to locate, and stray light can be minimized. The alternative of limiting the excitation bandwidth in conventional light sources results in a loss of photon flux and is much less desirable.

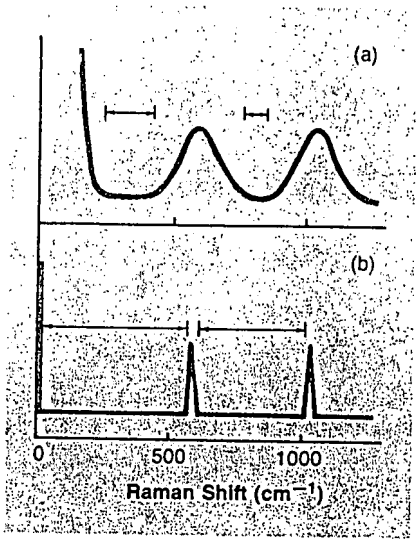

Figure 1. Stray light distribution in (a) a broad-band source at a 10-nm bandwidth, and (b) a monochromatic source. The available windows for fluorescence monitoring are substantially larger for case (b)

Temporal Resolution. Time-gating can be used to distinguish the fluorescence of the species of interest from the Rayleigh and Raman scattering of the eluant (*6*). The former has a finite lifetime after excitation while the latter is coincident with the excitation. The extent of rejection is determined by the fluorescence lifetime of the species divided by the laser pulse width or the photodetector response time, whichever is larger. It is clear that lasers are unique in being able to produce intense radiation in pulses short compared to fluorescence lifetimes, which are typically in the nanosecond range.

Polarization. Although conventional light sources in combination with polarizers can produce plane polarized light, with loss of half of the intensity, many lasers are inherently plane polarized because of the optical design. Since Rayleigh scattering and the stronger Raman lines are generally polarized, the suitable placement of the detector can lead to rejection of these undesirable signals.

Instrumental Design

The use of laser-excited fluorescence has lead to the detection of single atoms of sodium (*7*), so that signal levels are generally not a problem. The detectability is then limited by background noise levels, such as Rayleigh scattering (eluant and optical components), Raman scattering (eluant), and fluorescence (contaminants and optical components). The design of the flow cell to interface with HPLC is therefore critical. Cuvettes designed for 2π steradian collection of light (*8*) are well-suited for conventional light sources that cannot be focused to small spots, but offer no rejection of scattered light. The other design factors include small volume and proper imaging to the entrance slit of an emission monochromator.

An interesting concept for the elimination of stray light is based on suspending the flowing eluant in the form of a droplet (*9*). Figure 2a shows this arrangement, where the chromatographic eluant flows through a capillary tube and forms a droplet at the tip. A solid rod of appropriate dimensions comes in contact with the droplet from below, thereby maintaining the shape and size of the droplet under flow conditions. The obvious advantage is that no cell "walls" are involved. Scattering and fluorescence from optical components are thus reduced to a minimum. Very impressive results have been obtained in such a flow system (*9*). There are, however, a few problems with this design, all relating to the optical integrity of the droplet. Degassing of the eluant in HPLC is quite common, so that bubbles may be trapped at the tip of the capillary tube, seriously distorting the shape of the droplet. Etching a nick at the tip of the capillary tube lessens bubble formation, but does not eliminate it. Another type of distortion occurs in using different eluants with different viscosities and surface tensions, as is required in gradient elution schemes. The shape and size of the droplet change, thus introducing irreproducible changes in the focusing of the excitation laser and the imaging of the fluorescence onto the monochromator. Also, when the amount of laser light absorbed is substantial, including contributions from the nonfluorescing species, a phenomenon known as thermal lensing occurs (*10*).

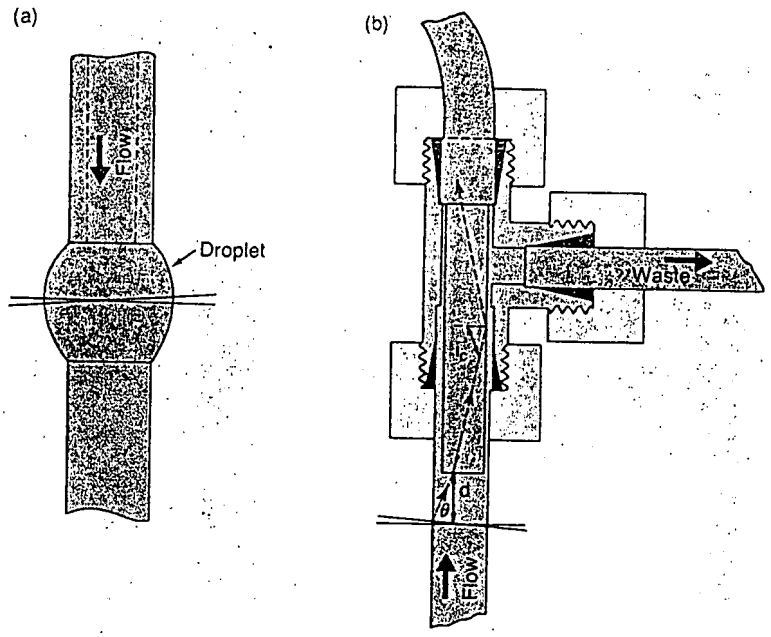

Figure 2. Two flow cells for laser fluorometric detection in HPLC. A flowing droplet suspended between a capillary tube and a solid rod (a). A capillary tube–optical fiber combination (b)

Again, proper imaging becomes a problem. Finally, the detector must be the last of a series since the flowing scheme essentially makes the technique destructive.

A capillary tube coupled with an optical fiber is an alternative (*11*), and is shown in Figure 2b. The chromatographic eluant flows upward and sweeps past the uncladded end of an optical fiber before going to waste. Any bubbles from degassing will tend to go around the optical fiber rather than be collected. Since the flow is guided by the capillary tube, changes in the physical properties of the eluant have little effect on the interaction region. The optical fiber can be placed very close to the focused laser beam to achieve a good collection efficiency. The unique feature here is that optical fibers transmit via total internal reflection along their length, so that a critical collection cone exists. Light rays entering the optical fiber at an angle greater than a certain angle θ will not be transmitted. This offers a convenient way to reject scattering and fluorescence originating from the walls of the capillary tube. From Figure 2b, it can be seen that transmission by the optical fiber occurs when

$$\sin \theta \leq (n_f^2 - n_c^2)^{1/2}/n_e \qquad (2)$$

where n_f, n_c, and n_e are the indices of refraction of the fiber, fiber cladding, and eluant respectively. It was found that the fluorescence signal is relatively insensitive to the position of the laser beam, presumably a result of an increase in the effective observation region to compensate for the decrease in collection efficiency as the distance d increases. The diameter of the output beam of the optical fiber (<1 mm) is ideal for coupling with a monochromator when placed at the entrance slit. To interface with small diameter chromatographic plumbing, it is only necessary to have a short region of larger diameter of the order of the optical fiber to accommodate the laser beam, and band spreading can be minimized. This design also allows the use as one of a series of detectors.

Yet another possibility is to use the sheath flow principle to confine the chromatographic effluent in the center of an ensheathing solvent stream under laminar flow conditions (*12*). The physical dimensions of the observation region are maintained to be constant but the effluent is isolated from the cell so that stray light from windows is reduced to a minimum. A minor problem with such a flow cell is that the exit channel must be of larger diameter so that peak broadening may occur unless this is used as the last of a series of detectors.

Detection limits in the low pg range have been demonstrated using each of these detector designs. The actual detection limit naturally depends on the species of interest, specifically the relative spectral locations of the absorption vs. emission wavelengths. The favorable systems have large red shifts in the emission bands, so that good filters cutting off the Rayleigh scattering and the fundamental Raman scattering of the eluant and optical components can be used. But the real advantage of laser fluorometry is realized when the red shifts are small, so that one has to use the "windows" in the eluant Raman emission to observe fluorescence, as explained in Figure 1. The fundamental limit is determined by the Rayleigh and Raman scattering efficiencies, which are typically 10^{-4} and 10^{-8}, respectively, that of fluorescence. For HPLC peaks distributed over an eluant volume of 1 mL, 1 pg is about the predicted limit (*5*). Smaller amounts can be detectable if microscale HPLC is used, in which case the small volumes afforded by laser-based detectors will make a substantial difference.

Two-Photon Excited Fluorescence

The simultaneous absorption of two photons by atoms or molecules to reach an excited state at the sum of energies of the two photons is a weak process. Using high power lasers, the absorption process is enhanced, and, using the high sensitivity associated with fluorescence monitoring, detection of species at concentration levels typical of HPLC becomes possible. One-photon and two-photon absorption are complementary processes in that they couple with a different set of excited states. This provides an added dimension for spectral selectivity in HPLC detection, so that overlapping spectral features in one case can become resolved features in the other. Selectivity is further enhanced by the fact that two-photon excited fluorescence is a more restrictive process. This can be seen from Figure 3. Normal fluorometric schemes (Figure 3a) require only two electronic states to be present, since both absorption and emission are allowed processes between states of different symmetries. Two-photon absorption (Figure 3b) occurs between states of the same symmetry, which implies that emission between the same two levels after excitation is forbidden. A third state of different symmetry must therefore be present. Emission can then occur between the initially excited level and this, or between this and the ground level after relaxation of the excited level to this level. The third level need not belong to another electronic state, because it can acquire the necessary symmetry properties by "borrowing intensity" from other electronic states by vibronic coupling. A third type of selectivity inherent to two-photon excited fluorescence is its dependence on photon polarizations (*13*). This exper-

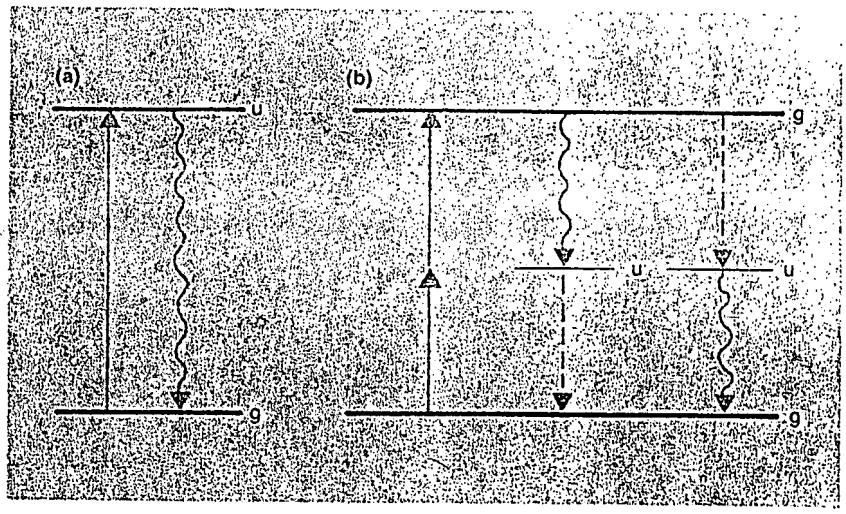

Figure 3. Transitions in (a) one-photon and (b) two-photon excited fluorescence. The same two states can participate in absorption and emission in case (a), but a third state must be involved in case (b). g and u are symmetry types. → absorption, ---→ relaxation path, and ⇝ emission

imental variable can be readily incorporated in the HPLC detector. Finally, the two-photon absorption process is resonantly enhanced when one of the photons matches the energy of a real molecular level. This is yet another variable that can be controlled to improve the selectivity of the detector.

The unusual selectivity of the two-photon excited fluorometric detector would naturally be of little value if the sensitivity were not at a useful level. Because excitation is typically accomplished with visible lasers while fluorescence is observed in the ultraviolet spectral region, stray light rejection is no longer a problem. Simple cut-off filters in series can reduce noise essentially to the dark-count level of phototubes without seriously degrading the signal. It can be shown that for a strong two-photon absorber with a cross section of 10^{-48} cm^4 s and a fluorescence yield of 0.5, a 4-W continuous laser (e.g., argon ion laser) focused to a 50μ spot yields 10^{11} fluorescence photons per second for a 1 μg/mL solution of a species with a molecular weight of 100. Including a factor of 10^{-3} for collection efficiency, optical losses, and phototube quantum efficiency, one should be able to detect a total amount of 0.1 ng spread out in a chromatographic peak of 1 mL. The use of pulsed lasers can lead to even more impressive results. A convenient choice is the 532-nm output of a doubled Nd:YAG laser. Commercial units can provide about the same average power but in pulses 10 ns long. The two-photon detectability can easily be improved by a factor of 10^3, even considering the poorer focusing properties of these lasers.

The instrumentation for two-photon excited fluorescence detection cannot be more simple. Some means of introducing the focused laser beam into the chromatographic flow stream is needed. Collection of fluorescence using cut-off filters and phototubes is no different from other fluorometric detectors. In fact, there is no reason

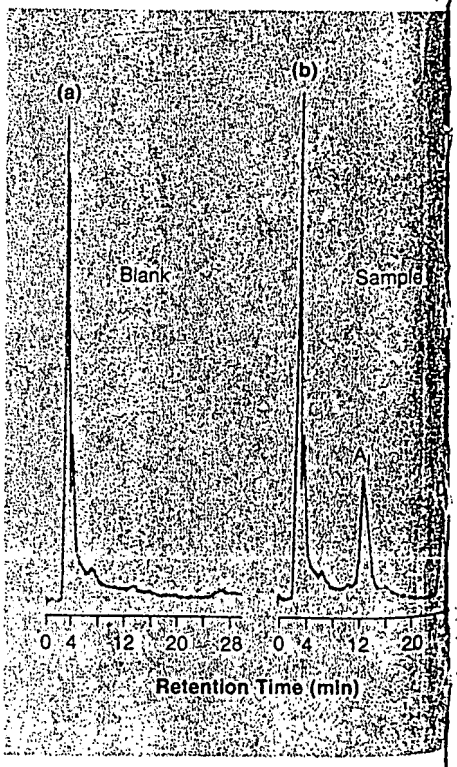

Figure 4. Determination of antitumor drugs A_1 and D_1 by direct injection of human urine. The blank (a) shows little interference during the elution of 63 pg each of the two drugs (b)

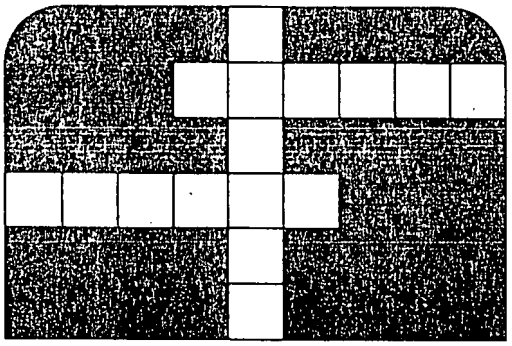

Lovibond®

PRECISION FUSED OPTICAL CELLS
■ COLOR MEASURING INSTRUMENTS
■ TINTOMETERS ■ COMPARATORS
■ WATER AND EFFLUENT TEST KITS
■ COLORIMETRIC CHEMICAL ANALYSIS EQUIPMENT ■ COLOR DISCS
■ ACCESSORIES AND ATTACHMENTS

now marketed in the United States by the new subsidiary of The Tintometer Limited of Salisbury, England.

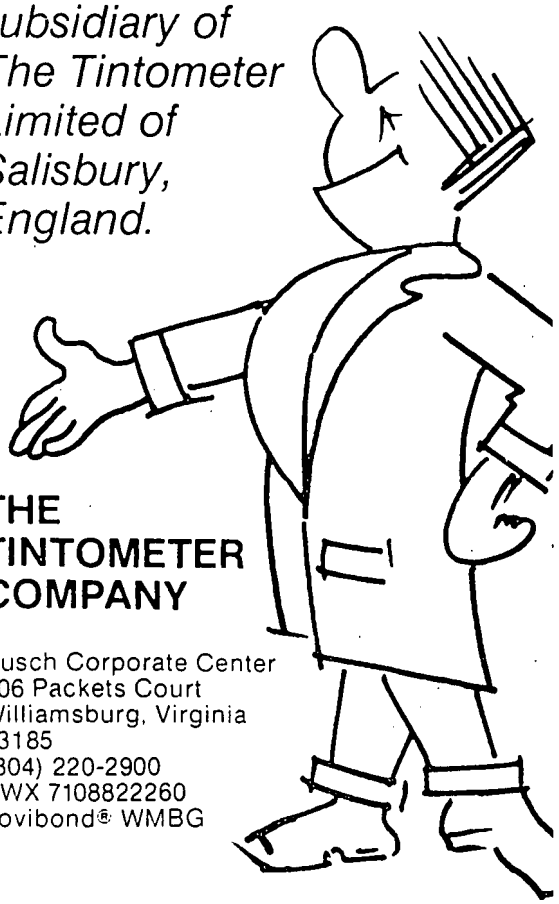

THE TINTOMETER COMPANY

Busch Corporate Center
206 Packets Court
Williamsburg, Virginia
23185
(804) 220-2900
TWX 7108822260
Lovibond® WMBG

CIRCLE 205 ON READER SERVICE CARD

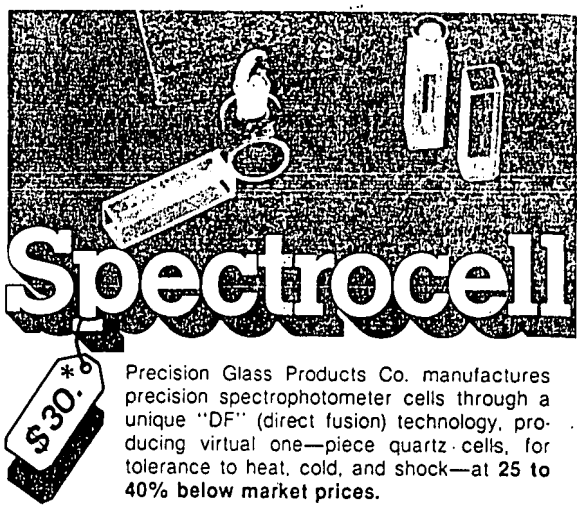

Precision Glass Products Co. manufactures precision spectrophotometer cells through a unique "DF" (direct fusion) technology, producing virtual one—piece quartz cells, for tolerance to heat, cold, and shock—at **25 to 40% below market prices.**

The highest quality

standard IR and UV quartz spectrophotometer cells

at the lowest prices

Send for our "Spectrocell" catalogue for a description of cells in stock, or send specifications for custom work. All cells are made in the U.S. and shipped in cushioned plastic boxes.

*1 cm. standard quartz cell

Precision Glass Products Co.
P.O. Box 145 Oreland, Pa., 19075
(215) 885-0145

CIRCLE 166 ON READER SERVICE CARD

Cancer— The Outlaw Cell

Richard E. LaFond, *Editor*

An estimated 390,000 Americans will die of cancer this year alone and one out of every four will develop some form of this dread disease within their lifetime.

Order from:
SIS/American Chemical Society
1155 16th St., N.W.
Wash., D.C. 20036

Statistics such as these show the need for a book that will explain our current state of the art in cancer research using simple, straightforward, non-medical language. *Cancer — The Outlaw Cell* successfully fulfills this need by making the latest advances in cancer research available to the general public in a clear, non-technical style that can be read and understood by both the professional scientist and non-scientist.

Written by leading experts at the forefront of their specialties and profusely illustrated in color, this collection of articles covers the great strides that have been made in understanding the causes of cancer, how this disease is spread, cancer as a biochemical problem, and non-surgical modes of therapy.

CONTENTS

192 pages (1978) clothbound $15.00
LC 78-2100 ISBN 0-8412-0405-5
192 pages (1978) paperback $8.50
LC 78-2100 ISBN 0-8412-0431-4

EVERY LINDE CUSTOM GAS MIXTURE EXPERT HAS OTHER EXPERTS BEHIND HIM.

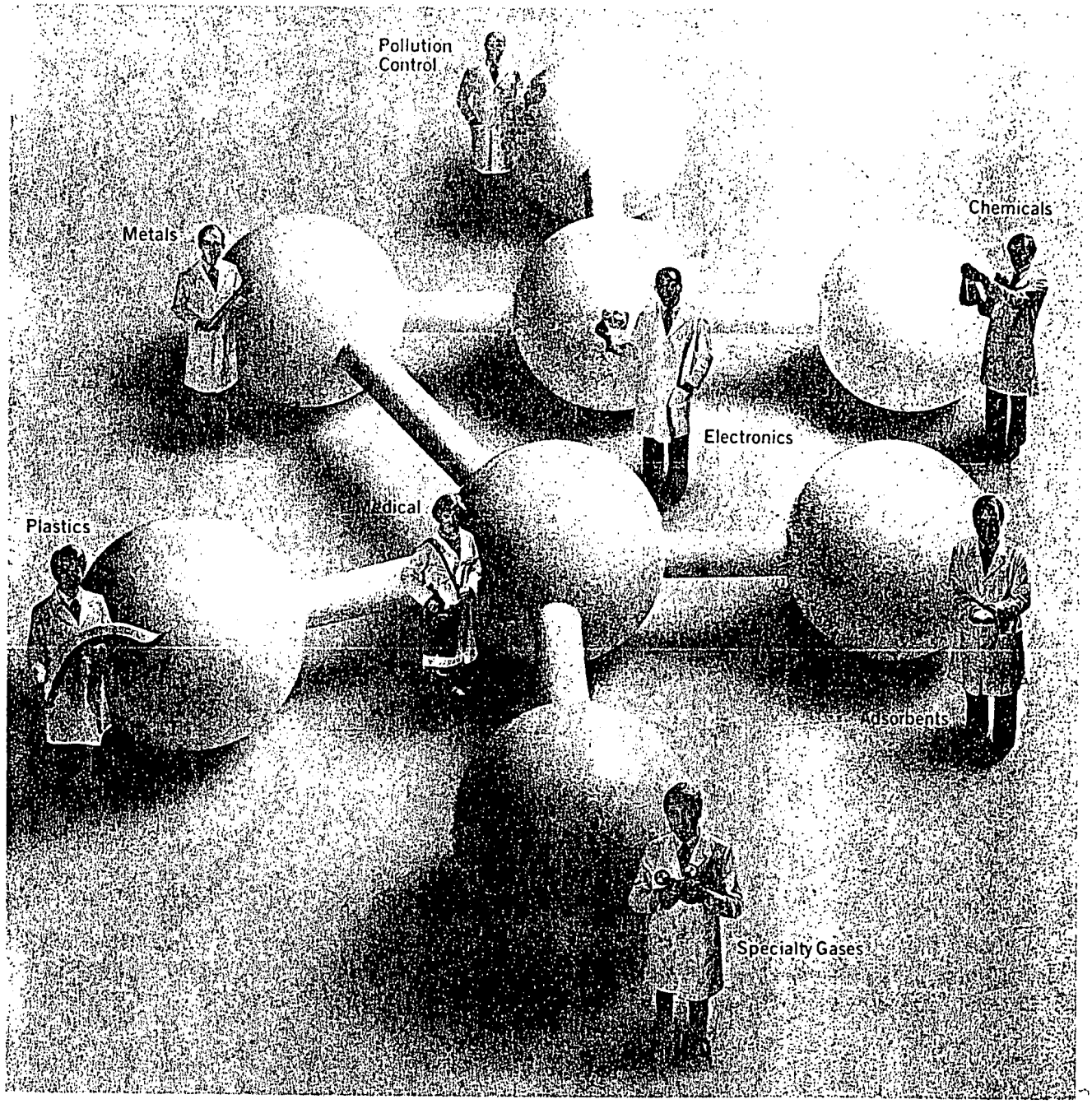

Whatever your field of work is, there are experts at Union Carbide we can consult in order to advise you regarding your needs and to assure that you receive the Custom Gas Mixture that is best for your application.

Linde prepares your custom-gas mixtures with the precise gas purities and proportions, in the exact volume you specify. We are the most experienced gas supplier in the country. Our laboratory analytical facilities are the most advanced in the industry. And our access to Union Carbide's scientific resources importantly enhances our ability to serve your interests.

For more information, write or phone: Union Carbide Corporation, Linde Division, National Specialty Gases Office: 100 Davidson Ave., P.O. Box 444, Somerset, NJ 08873. Telephone (201) 356-8000. TWX 710-997-9550.

UNION CARBIDE LINDE SPECIALTY GASES & RELATED PRODUCTS

TAKE THE GUESSWORK OUT OF YOUR GAS WORK.

CIRCLE 214 ON READER SERVICE CARD

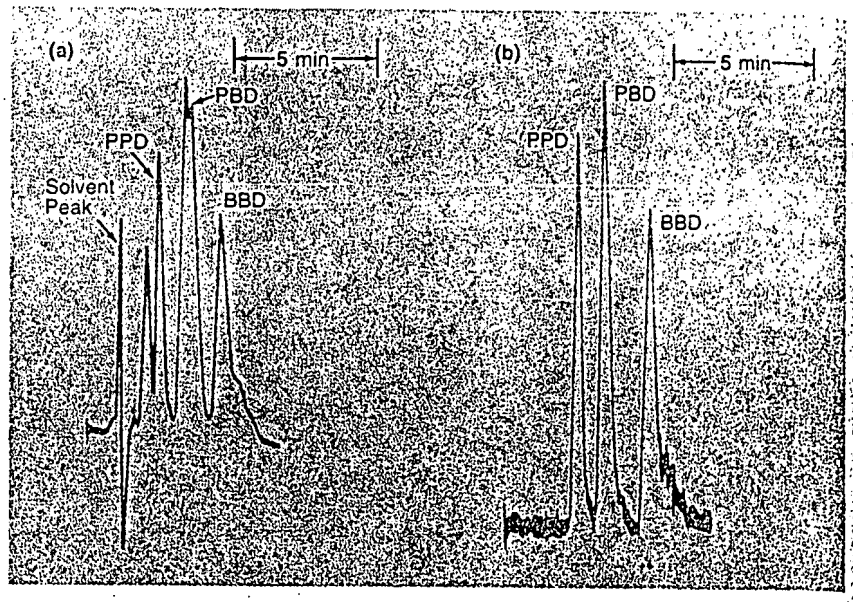

Figure 5. Simplification of chromatograms by two-photon excited fluorimetry. All seven compounds in a mixture show up and interfere with one another in a standard UV absorption detector (a), while only the oxadiazoles appear in the two-photon detector (b)

why the same laser beam cannot be used to excite both one- and two-photon states, simultaneously gathering the two types of information through separate filter/monochromator combinations.

Applications

The high sensitivity of laser fluorometric detectors has been demonstrated in the determination of pg levels of each of the four aflatoxins (B_2, B_{2A}, G_2, and G_{2A}) (*9*). There, a modulated He-Cd laser at 325 nm excites visible fluorescence from the four species in a spectral region well beyond the fundamental Raman scattering. The forms B_{2A} and G_{2A} are the corresponding fluorescing derivatives of the more important, naturally occurring forms B_1 and G_1. The detection limit is about 2 ppb of B_1 in corn samples, due to other interferences.

The use of laser fluorometric detection in the study of biological fluids has been reported (*11*) for the antitumor agents adriamycin (A_1) and daunorubicin (D_1). A 20-μL sample of human urine is injected directly and separated by reversed phase HPLC coupled to an optical-fiber-based fluorometric detector. Figure 4 shows the chromatograms of a urine blank and a urine sample spiked with 63 pg (total amount) each of A_1 and D_1. Detection in the 10-pg range with no noticeable interference is achieved. The unique aspect is that visible laser at 488 nm is used to excite visible fluorescence at 590 nm. The complex chromatograms normally associated with the HPLC of untreated urine using either UV absorption or UV fluorescence are avoided. The use of a laser has improved the signal-to-noise level sufficiently to deal with these low concentration levels, typical of patients receiving such drug treatment. It is also found (*14*) that interference-free determinations at comparable concentration levels are possible in unextracted human blood serum. There, however, chemical changes to the drugs do occur in time so that more careful controls are necessary.

The unique features of a two-photon excited fluorometric detector have been demonstrated in the separation of three oxadiazoles (*15*). Simplification of the chromatogram in the analysis of a mixture of compounds that normally are not resolved using UV absorption or fluorescence is illustrated in Figure 5. An interesting application is in the study of biological fluids by HPLC. Normal human urine and blood plasma, although they are complex mixtures, do not show any signal in two-photon excited fluorescence, even at high sensitivity settings (*14*). Drugs such as A_1 and D_1, however, show good two-photon response and can be detected at the 10-ng level with a 2 W argon ion laser by direct injection of untreated samples. The use of pulsed lasers should give even better results.

The striking selectivity that is offered by laser fluorometric detectors makes them invaluable for complex samples. Chromatograms are simplified yet the injected amount can remain small due to the high sensitivity. One of the most complex samples is the coal-derived liquids. Literally thousands of different compounds are

present, each at trace levels. The presence of large molecules and highly conjugated π-electronic systems makes fluorometric detection applicable. The asphaltene fraction of coal liquid is injected in 40-μg total quantities for reversed phase separation by a 10μ C_{18} column using a 50:50 acetonitrile:water to 100% acetonitrile gradient. By putting the optical-fiber flow cell in series with a commercial UV detector at 254 nm, one can simultaneously obtain the UV absorption, one-photon visible fluorescence, and two-photon excited UV fluorescence in a three-dimensional chromatogram (*14*). A typical set of three chromatograms is shown in Figure 6. It should be noted that the chromatograms are reproducible and that the noise levels in each are insignificant on the corresponding scales.

The first observation is that baseline resolution is not achieved. This is due to the high complexity of these samples and the inability of the chromatography to properly resolve the components. But, the three detectors together provide information that is much more useful than each of the detectors individually can provide. The

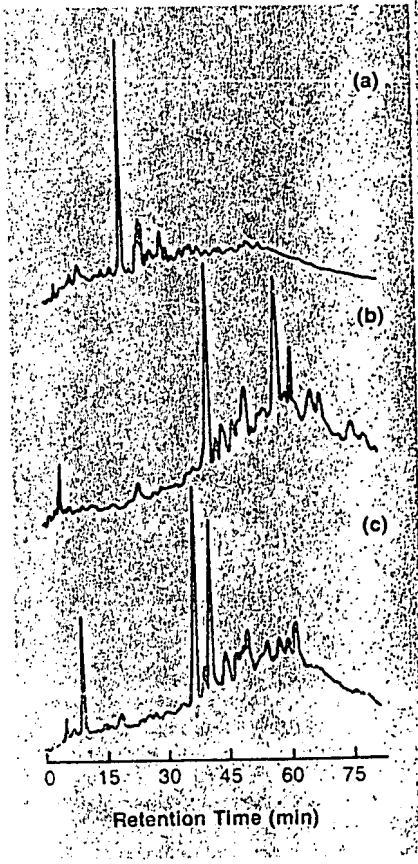

Figure 6. Three-dimensional chromatogram of the asphaltenes: (a) UV absorption at 254 nm; (b) 540-nm fluorescence excited by 488-nm laser; and (c) > 350-nm fluorescence excited by two-photon absorption of 488-nm laser

second observation is that the bulk of the species appears earlier in the UV chromatogram (about 35 mins) compared to the other chromatograms (about 50 mins). This is consistent with the separation by reversed phase columns, where the smaller molecules are eluted earlier than the larger molecules. The visible fluorometric detector favors large, conjugated molecules and does not respond to the smaller molecules that have the lowest excited electronic state in the UV region. The two-photon process should excite molecules to energies equivalent to a photon at 244 nm, but the largest response occurs when the process is resonantly enhanced in the presence of low-lying electronic states. These low-lying states are again characteristic of the larger, conjugated molecules. The third observation is that visible fluorescence is monitored at 540 nm, only 1973 cm^{-1} from the excitation wavelength of 488 nm. This is in the heart of the fundamental Raman scattering region, and only the light rejection offered by a monochromatic excitation source makes the study possible. The fourth observation is that many compounds show two-photon excited fluorescence even though it is a more restrictive process. More important is that it clearly provides somewhat different information than visible fluorescence, and this can help in the identification of the compounds. Results in the use of these chromatograms for the classification of coal-derived liquids will be published later (*16*).

Summary

Lasers have brought new directions in fluorometric detectors for HPLC by improving selectivity and sensitivity. The most encouraging aspect is that extremely sophisticated lasers are not needed, and standard lasers associated with normal Raman instruments can be used both for one-photon and two-photon excitation. As HPLC strives for higher and higher resolution, the small detector volumes offered by lasers will become increasingly important. And, as interests surge in complex environmental and clinical samples, lasers will probably strengthen their hold as an integral part of any multidimensional chromatographic study.

Research support of the work leading to this manuscript is derived from the Director of Energy Research, Office of Basic Energy Sciences. WPAS-KC-03-02-03. The Ames Laboratory is operated for the U.S. Department of Energy by Iowa State University under Contract No. W-7405-Eng-82.

Literature Cited

(1) Worthy, W. *Chem. Eng. News* 1978, July 31, 28.
(2) Mack, G. D.; Ashworth, R. B. *J. Chromatogr. Sci.* 1978, *16*, 93.
(3) Saner, W. A.; Fitzgerald, G. E.; Welsh, J. P. *Anal. Chem.* 1976, *48*, 1747.
(4) Anders, D. E.; Robinson, W. E. *Geochim. Cosmochim. Acta* 1977, *35*, 661.
(5) Yeung, E. S. "Lasers and Chemical Analysis," Hieftje, G. M.; Lytle, F. E.; Travis, J. C., Eds.; Humana: Clifton, N.J., 1980; in press.
(6) Friedman, J. M.; Hochstrasser, R. M. *Chem. Phys.* 1974, *5*, 155.
(7) She, C. Y.; Prodan, J. V.; Pan, C. L.; Fairbank, W. M. American Chemical Society Meeting, Houston, Tex., 1980, paper No. 63. Gelbwachs, J. A. American Chemical Society Meeting, Houston, Tex., 1980, paper No. 90.
(8) For example Model FS-970 detector, Schoeffel Instruments, Westwood, N.J.
(9) Diebold, G. J.; Zare, R. N. *Science* 1977, *196*, 1439.
(10) Long, M. E.; Swofford, R. L.; Albrecht, A. C. *Science* 1976, *191*, 183.
(11) Sepaniak, M. J.; Yeung, E. S. *J. Chromatogr.*, 1980, *190*, 377.
(12) Hershberger, L. W.; Callis, J. B.; Christian, G. D. *Anal. Chem.* 1979, *51*, 1444.
(13) McClain, W. M. *J. Chem. Phys.*, 1973, *58*, 324.
(14) Sepaniak, M. J. Ph.D. Thesis, Iowa State University, Ames, Iowa, 1980.
(15) Sepaniak, M. J.; Yeung, E. S. *Anal. Chem.*, 1977, *49*, 1554.
(16) Sepaniak, M. J.; Yeung, E. S., to be published.

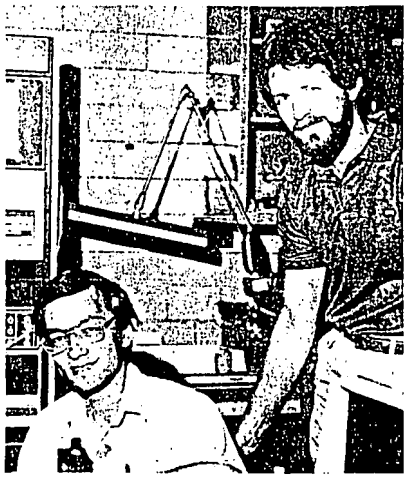

Ed Yeung (left) received his AB from Cornell University in 1968 and his PhD from the University of California at Berkeley in 1972. He is currently associate professor of chemistry at Iowa State University where his research interests include new optical methods of analysis, pattern recognition techniques, high resolution spectrometry, photochemistry, and nonlinear optical phenomena. Mike Sepaniak received his BS from Northern Illinois University in 1974. He is currently a graduate student at Iowa State University and will be joining the department of chemistry at the University of Tennessee as assistant professor starting in January 1981.

CIRCLE 144 ON READER SERVICE CARD

Reprinted from Analytical Chemistry, 1992, 64.

Interactive Control of Pulsed Field Gel Electrophoresis via Real Time Monitoring

David A. McGregor and Edward S. Yeung*

Ames Laboratory-USDOE and Department of Chemistry, Iowa State University, Ames, Iowa 50011

The migration of DNA fragment bands through a slab gel can be monitored by UV absorption at 254 nm and imaged by a charge-coupled device (CCD) camera. Background correction and immediate viewing of band positions to interactively change the field program in pulsed-field gel electrophoresis is possible throughout the run via this detection scheme. The use of absorption removes the need for staining or radioisotope labeling, thereby simplifying sample preparation and reducing hazardous waste generation. This leaves the DNA in its native state and further analysis can be performed without destaining. The optimization of buffer concentration, electric field strength, temperature, agarose concentration, as well as pulse duration can considerably reduce total run time. For example, DNA from 2 to 850 kb can be separated in 3 h on a 7-cm gel with interactive control of the pulse time, which is 10 times faster than using a constant field program.

INTRODUCTION

Major advances have been made in the human genome project, as can be witnessed by the current achievement of complete sequencing of one chromosome of the yeast, *Saccharomyces cerevisiae*, of about 300 kilo(base pairs) (kb) (*1*). Still, to map and sequence the entire human genome, which is 24 chromosomes with 3×10^9 base pairs (bp), this current achievement is 4 orders of magnitude short. To ultimately achieve this goal, critical reevaluation of the current techniques used to map the genome must be done. The methods currently used are (2) (1) family studies, genetic maps, which are large databases of family histories and trends; (2) ordered libraries, physical maps, of large DNA fragments (hundreds of kilo(base pairs) from chromosomes to allow mapping of the individual genes, usually separated by pulsed field gel electrophoresis (PFGE); (3) digestion of the larger fragments into smaller and separation, usually done by dc field gel electrophoresis; and (4) sequencing of the smaller fragments into the constituent A (adenine), T (thymine), C (cytosine), and G (guanine) bases, which are done by slab gel or more recently by capillary electrophoresis (*3*). This article will center around the separation of large fragments of DNA.

dc field gel electrophoresis can separate fragments up to ~30 kb directly on the basis of the size to mobility ratio. Above this size the separation mechanism breaks down and the fragments will not separate because they can no longer effectively "sieve" through the gel. To alleviate this problem, another mechanism is introduced by pulsing the electric field. When the electric field is applied in two directions alternately, the fragments reptate, or snake through the gel and separations into the mega(base pairs) (Mb) can be performed. PFGE was first demonstrated in 1984 (*4*). As opposed to dc electrophoresis, PFGE alternates the electric field at a predetermined angle (Figure 1). There are many configurations currently being utilized (*5, 6*). One such reliable configuration is the contour-clamped homogeneous field (CHEF) device (*7*). In the CHEF apparatus the electric fields are applied at 120° angles and the apparatus is horizontal. By switching the electric field for some predetermined time, the fragments will zigzag down the length of the gel. The CHEF apparatus separates fragments with reasonably straight lanes and offers an open design.

The separation mechanism of PFGE is not well understood, and several theories have been proposed (*8–12*). PFGE has the capability of separating DNA fragments from the kilo(base pair) level to above 6 Mb. When restriction digests are performed on unmapped chromosomal DNA the resultant fragments are of unknown size and quantity. The choice of pulse length is critical to optimal separation of these fragments. Selection of pulse length is usually an "educated guess" based on the estimation of fragment sizes produced and the running conditions. Electrophoresis must be performed and the gel stained before the results of the separation are known. If the fragments were not separated then another run must be performed with different parameters. When PFGE takes from 10 h to days to perform, the time spent in optimization can add quickly. However, if DNA migration through the agarose is monitored in real time, the pulse length can be adjusted to optimize the separation as the fragment sizes become apparent. This reduces the number of experiments required for optimal separation of chromosomal DNA fragments. Monitoring of fragments as they migrate allows for separation and identification over a wide range of sizes in a single run.

In this work, we demonstrate the advantages of interactive control in PFGE. Real time monitoring of the separation is possible using UV absorption and CCD (charge-coupled device) imaging (*13*). The optimal separation condition can be arrived at in a systematic fashion. The final result is a substantial reduction in the separation time compared to constant field programming approaches.

EXPERIMENTAL SECTION

Apparatus. The apparatus shown in Figure 1 consists of the CHEF design made in-house from blueprints supplied by Chu et al. (*14*). The power supply and pulse controller were purchased from Bio-Rad Laboratories. For cooling, a pump (Cole-Parmer Model 7520-00) recirculates the running buffer through Tygon

0003-2700/92/0364-0001$03.00/0

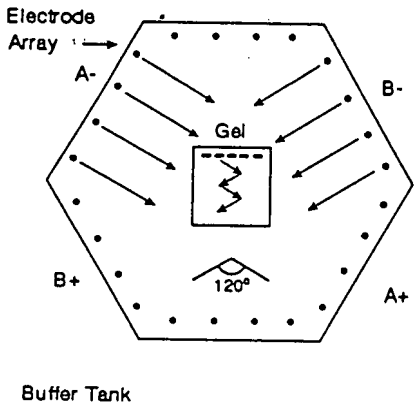

Figure 1. Schematic diagram of a contour-clamped homogeneous electric field apparatus (CHEF). Voltage is applied at the A electrodes then switched to B at some predetermined pulse time. Pulses are applied at 120° angles to each other. Buffer is recirculated and cooled through a Tygon tube immersed in a constant-temperature bath.

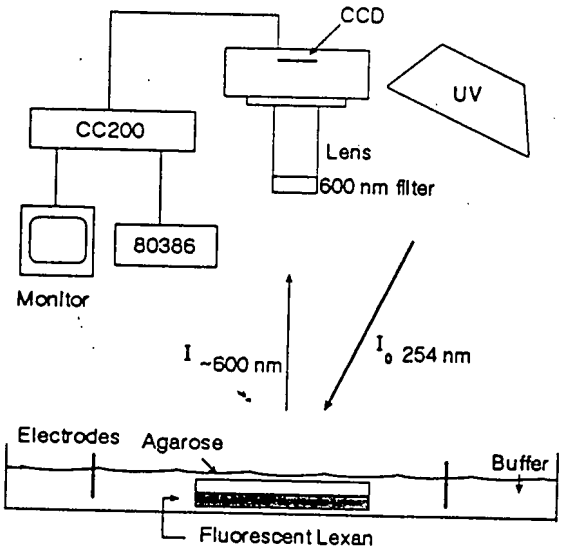

Figure 2. Schematic diagram of experimental setup. UV light illuminates the gel. As the UV light passes through the gel, the DNA fragments will absorb some of the radiation. The remaining light strikes the lexan plate and is reemitted as fluorescence to be imaged by the CCD. To achieve true absorbance, a background image is taken before the voltage is applied and all subsequent images are divided by this blank image. Key: UV, 254 nm UV lamp; 600-nm filter, 600-nm 80-nm band-pass filter; lens, focuses images onto CCD; CCD, charge-coupled device; CC200, dedicated data array for image storage; 80386, PC for electronic storage of images; monitor, for hard copy and visual analysis of separation.

tubing contained in a constant-temperature bath.

The agarose gel is illuminated only during imaging by a 30-W UV lamp (Cole-Parmer) operating at 254 nm which is mounted 60 cm above the gel. The imaging system consists of a scientific grade CCD (Thomson TH7882 576 × 384 pixel) thermoelectrically cooled to −40 °C (Photometrics Ltd.). The focusing lens is a 90 mm *f*/2.5 telemacro (Tamron Co.) which has flat-field focusing properties at low aperture. The flat-field lens allows full focusing across the entire imaged area. A 600-nm, 80-nm band-pass filter is used to reject the direct illumination from the lamp and any stray light from the room. The CCD is 75 cm from the agarose. The entire experimental apparatus is shown in Figure 2.

Images shown were 3.0 s each for 16 individual exposures. An exposure filled the individual pixels to roughly 90% capacity. The 16 frames were averaged together to further reduce the shot-noise limitations of the CCD. Total illumination time per image (every $^1/_2$ h) for the gel and DNA was around 3 min. This UV exposure time was not sufficient to damage the DNA for this experiment. When the gel is imaged, the running buffer is static and the applied voltage is off. All two-dimensional data taken from the gels are analyzed by taking the average of 35 pixel rows across each lane, as shown in Figure 3.

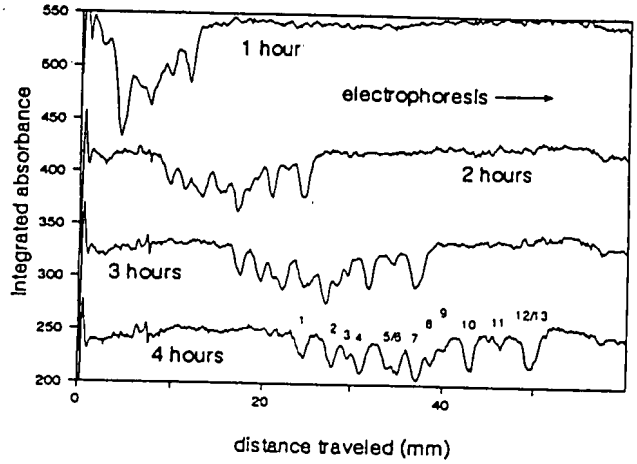

Figure 3. Separation of high molecular weight markers. Note the negative peaks indicating UV absorbance. A total of 35 pixels have been averaged across one lane. Conditions: 6 V/cm, 0.9-s pulse, 10 mM TPE buffer, 12 °C, 16 frames averaged, 0.5% agarose, and 210 ng of DNA total injected. DNA fragments are 48.5, 38.4, 33.5, 29.9, 24.8, 22.6, 19.4, 17.1, 15.0, 12.2, 8.6, and 8.3 marked from 1 to 13, respectively.

Since the absorption bands of the DNA are around 5% or less, the inhomogeneities in the gel and the fluorescent background must be reduced to allow proper visualization. This is accomplished by taking an image prior to applying the electric field and storing it in the CCD memory buffer (CC200). All subsequent images are normalized relative to this blank image, thereby reducing much of the systematic noise. This type of imaging is called flat-fielding. The subsequent images can be sent to a monitor for immediate analysis or to a PC for electronic storage for later data workup. Photodocumentation of the gels were taken off the monitor by a 35-mm camera.

DNA. The DNA used in this research consists of Lambda DNA digested by *Hin*dIII (lot 9PD114) from Bethesda Research Laboratories as a marker from 560 bp to 23.1 kb. High molecular weight marker (HMW) from BRL (lot AEH703) is a marker from 8.3–48.5 kb. All chromosomal DNA was purchased from Promega. The *Moraxella bovis* (lot L31) (3.1 Mb) was digested with both *Not*I (lot 02302) (8 base recognition site) and *Csp*I (lot 01740) (7 base recognition site). The *Staphylococcus aureus* (3.1 Mb) (lot L21) was digested with *Csp*I. The chromosomal digestions were performed as per the protocol from Promega and then allowed to equilibrate in the running electrophoresis buffer for 45 min prior to separation.

The chromosomal DNA is supplied in 1.6 mm diameter strings of agarose which are cut to 5-mm lengths. Digest of the *M. bovis* with *Not*I is first equilibrated with the restriction enzyme buffer for 30 min on ice. Then the enzyme [5:1 enzyme (units):DNA (μg)] and bovine serum albumin (BSA) is added and allowed to equilibrate for 30 min on ice to allow the enzyme to completely pervade the agarose plug. The digest is performed at 37 °C for 3 h and the reaction quenched by adding EDTA to 50 mM. Digestion of *M. bovis* and *S. aureus* with *Csp*I is equilibrated as before, and then the enzyme (8:1) is added with BSA and equilibrated. The digestion is performed at 30 °C for 5 h.

Gel. The 0.5% (w/w) agarose (FMC Fast Lane lot 11509) was melted and poured between the fluorescent lexan base and a quartz plate with 4-mm spacers and allowed to set for 30 min at room temperature. The wells were formed with a Teflon comb 5 mm wide by 1.5 mm thick and 4 mm deep.

The 10 mM TPE (THAM, Phosphoric acid, EDTA) running buffer for electrophoresis consisted of 7.86 mM THAM [tris-(hydroxymethyl)aminomethane], 2.07 mM phosphoric acid and 0.07 mM EDTA (ethylenediaminetetraacetic acid) at pH 7.75. The pH of the buffer did not significantly change after 3–6 h of electrophoresis. The running buffer was poured to a depth approximately 4 mm over the top of the agarose slab for enhanced cooling.

The quartz plate was then removed and the HMW and λ *Hin*dIII was injected with a 5-μL pipet. The chromosomal DNA

was cut into 5-mm lengths prior to digestion and was inserted as a plug of agarose into the slab gel. The agarose plug allows handling of the large DNA fragments without shearing or damaging of the DNA.

Separations. The optimized separation took 3 h with a dynamically adjusted pulse sequence. At 12 V/cm or 333 V the current was 250 mA and 70 W of power was dissipated. Pulse sequence was 0.6 s for 1 h, then 3.0 s for 1 h, and then 6.0 s for 1 h. Other separations shown are for static pulses for up to 6 h to show the lack of complete separation in the system.

RESULTS AND DISCUSSION

The purpose of this work is to achieve the fastest separation of DNA fragments over a wide range of sizes in an unknown sample. The size range being considered is from 560 bp to 850 kb. This range is important in the mapping of the human genome (*15*) and has proven utility in forensic applications involving DNA fingerprinting (*16*). The critical point is that fragments resulting from cutting a given DNA by restriction fragments do not have predictable sizes. Even though statistical considerations can provide an estimate of the number and rough sizes of the set of fragments, there is always the possibility that important information will be missed if a generic recipe is used for electrophoresis. Some of the parameters for electrophoresis are relatively easy to select, such as buffer composition, applied voltage, temperature, and agarose concentration. These will first be optimized for the test system. One is then left with the control of the pulse forms in CHEF. These will be interactively adjusted during the separation to achieve adequate resolution at the maximum speed for a given sample. To demonstrate this concept, we have used different DNA digests to cover the 1000X size range in different lanes on one slab gel. This is necessitated by the lack of available standards that will form a good test case and to avoid cross-interactions between the DNA fragments which will affect the integrity of the size standards.

Buffer Composition. Buffer type and concentration affect the separation time. Many PFGE buffers have concentrations on the order of 100 mM. This research constitutes a reduction of buffer concentration by 10–20-fold (*17*) and produces a marked increase in mobility. In this case the reduction of running buffer concentration does not adversely affect the DNA or separation. Further reduction in the buffer may have adverse effects on the separation because of denaturation of the DNA or activate enzymes or other contaminants that may lyse the DNA strands much as the restriction enzymes do. There is no evidence for this occurring in these separations because of the sharp bands, which would otherwise be smeared if the forementioned problems were present. Other buffer compositions could increase the mobility, thus decreasing separation time, but were not investigated in this work.

Applied Voltage. Another parameter involved in decreasing the separation time is the potential gradient. Standard potential gradients for PFGE on chromosomal DNA fragments range from 3 to 10 V/cm. In principle, higher voltages will increase the migration velocities. However, voltages higher than this can present other problems in separation. Joule heating can become important even with circulation, leading to band distortions (*18*). The higher voltages will also lead to trapping of the DNA in the gel. Trapping at higher voltages has been demonstrated previously (*19, 20*). Trapping is the phenomenon where larger fragments cannot travel through the agarose or becomes hung up on the pores because Brownian motion cannot overcome or unhook the DNA strands when the force of the electric field is too strong. It appears that an 850-kb fragment is severely attenuated in one lane of some of our gels, most probably due to the intermittent removal of the electric field during visualization. When the field is reapplied, some DNA remains behind where the compression zone was last imaged. Lower voltages or decreased agarose concentration can partially correct this problem. In these separations the field is 12 V/cm.

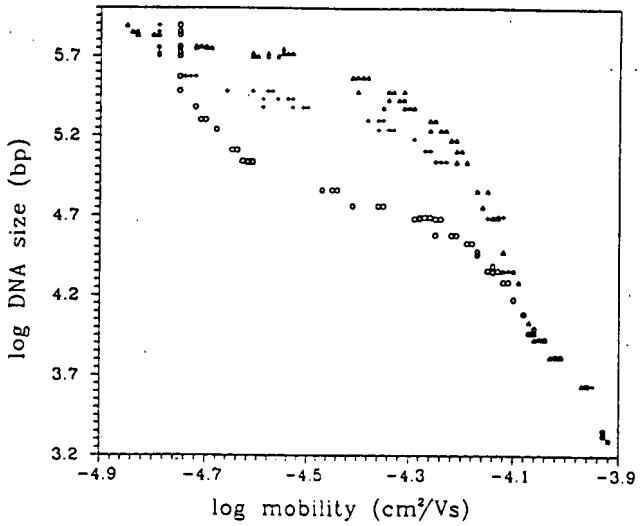

Figure 4. Graph of mobility vs DNA size. The three curves represent mobilities of DNA (cm^2/Vs) as a function of pulse width. Note the independence of pulse time on the mobilities at DNA sizes below 20 kb. The plateaus show the wide range of mobilities for relatively small regions of DNA sizes. At higher fragment sizes there is no change in mobility for the 0.6- and 3.0-s pulses, indicating the compression zone. Data are from three static separations using 0.6-s (O), 3.0-s (+), and 6.0-s (Δ) pulses. Other conditions: 12 V/cm, 30 °C, 0.5% agarose, 10 mM TPE buffer, 16 frames averaged.

Temperature. Most separations of this nature are run at 4–10 °C. This low temperature is required due in part to the length of the separation and the severe ohmic heating by the higher buffer concentrations normally used. The separations here are performed at 30 °C. The problem often encountered at higher temperatures is denaturation of the DNA above their critical temperature (T_m). Once again this is not a problem here, as the T_m values for these chromosomal DNAs are around 43 °C. The pH (7.75) change is not significant between 24, where the buffer is made, and 30 °C, where the separation is run. The increase in mobility from 15 to 30 °C is found to be almost a factor of 2.

Agarose Concentration. The agarose concentration for these experiments is 0.5% (w/w). This is not extraordinary for PFGE separations but normal concentrations are around 0.75–1.5%. Lower concentrations would speed the separation in general. Lower gel concentrations would make the agarose very hard to manipulate, but in this setup the gel remains stationary throughout. Lower agarose concentrations can also help to reduce trapping of the DNA by the pores because of the larger pore sizes. Ultimately, the requirement for adequate gel strength would limit the decrease in gel concentration.

Separations. The separation, as it occurs, is monitored by illumination of the gel with UV light. Typically, at the $^1/_2$-h mark, the smaller fragments have moved away from the darker band which is closer to the wells. This darker band has all the remaining fragments and is called the compression zone (CZ). This zone has a wide range of DNA fragments that are all moving through the gel with the same mobility. Almost all the constant pulse separations have compression zones whether they are behind the main separation area or in front or both. This demonstrates the need for different pulse times to optimally separate the full range of fragments.

Figure 4 shows the mobilities of the fragments in three different runs where the pulse times are kept constant. Note the plateau regions where the mobilities are relatively wide ranging for the DNA sizes involved. This shows good separation for this range of fragments at this particular pulse time. The three individual plots in Figure 4 converge at lower

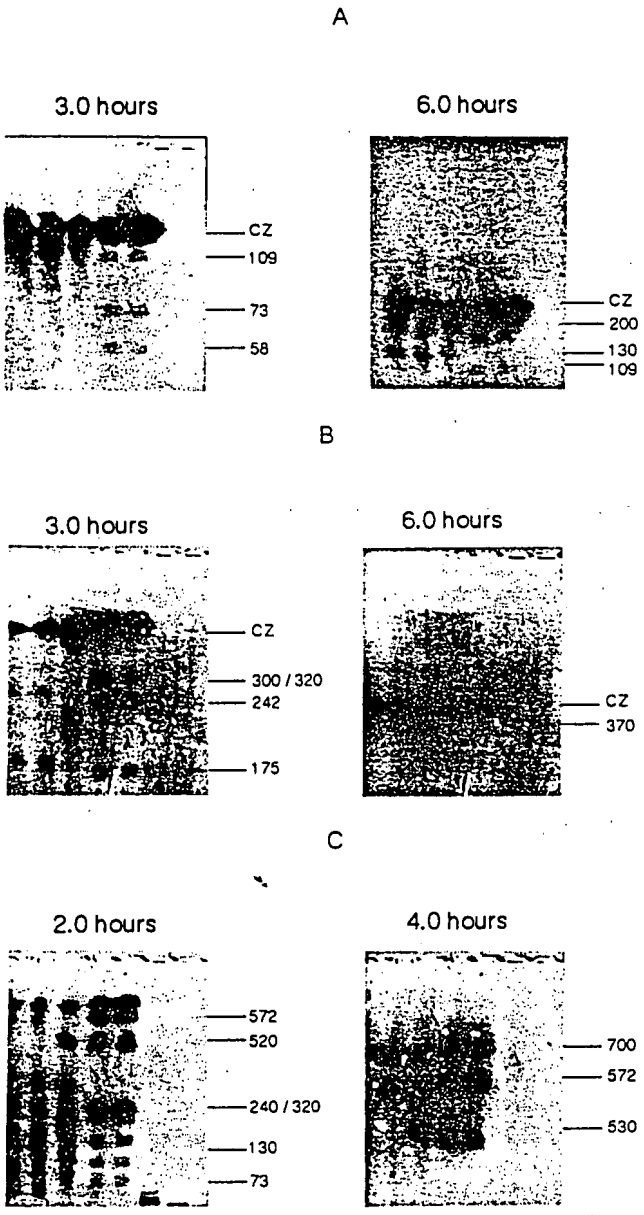

Figure 5. Three separations using static pulses; 0.6-s pulse for 3 and 6 h, 3.0-s pulse for 3 and 6 h, and 6.0-s pulse for 2 and 4 h. Digestions from left to right: lanes 1 and 2, *M. bovis Csp*I; 3, *M. bovis Not*I; 4 and 5, *S. aureus Csp*I; 6, high molecular weight markers (270 ng); 7, λ *Hin*dIII (180 ng). Amount of chromosomal DNA loaded into the gels is 1–2 μg. Other conditions: 12 V/cm, 30 °C, 0.5% agarose, 10 mM TPE buffer, 16 frames averaged. Note that resolution is not achieved above 200 kb for the 0.6-s pulse even after 6 h. Resolution is not adequate in the 3.0-s static pulse above 370 kb, and some resolution is lost at the lower sizes as well. For the 6.0-s pulse the middle range (240 and 320 kb) is not resolved and marked loss in resolution at lower DNA sizes is noted although the largest fragments are well separated within 4 h.

fragment sizes. This shows the independence of the mobilities on pulse time for smaller fragments, demonstrating contribution primarily from a sieving mechanism for these smaller fragments. At this particular set of conditions, the convergence limit is around 20 kb. The upward trend of the plots at lower mobilities shows the start of the CZ, where the pulse length is not sufficient to separate the fragments.

Figure 5 shows results of constant-pulse separations, showing the lack of separation at those particular pulse times. Even at 6 h the separations are not complete. This demonstrates the need for modification of pulse times during the separation. Ideally, one would continuously alter the pulse times during separation so that the plateaus in Figure 4 keep moving up to maximize resolution. We note that the three pulse times displayed in Figure 4 provide well-spaced plateaus already, and a finer dynamic modification is not necessary.

The protocol is as follows. A given pulse time is selected and the separation is monitored at regular intervals. As soon as the lower molecular weight fragments begin to move away from the compression zone, even though the complete separation of all fragments in that range is not achieved, the next pulse time is selected. This is because one can anticipate further separation of the lower molecular weight bands when the next longer pulse time is in effect. When the intermediate sizes of fragments begin to separate from each other, the final pulse time can be selected. The electrophoresis will continue under this pulse time until final separation is observed in the image. Exactly when the pulse times are changed depends on the size range of the fragments in the particular sample and on the proximity of the bands in each size range. This must be done interactively. In this work, the operator decides on the parameters by following the separation in real time. There is no reason why this decision process cannot be converted into an "expert system" to achieve full automation. For example, the CCD image can be analyzed as in Figure 3 and standard chromatographic "resolution" indicators can be used to judge the separation performance at every stage.

Figure 6 shows the results of a separation of DNA fragments with interactive control of the pulse times via real-time monitoring. After the selection of the buffer composition, temperature, voltage, and agarose concentration, the optimal dynamic pulse times were arrived at during the very first trial. In preliminary runs the temperature was much lower and the total optimized separation time was 6 h. This shows the clear advantage of interactive control.

The bands of DNA for the chromosomal DNA used here have been previously determined (*21*, *22*). The higher resolution of this separation has resulted in several doublets from 48 to 175 kb in the *S. aureus Csp*I digest. There are at least three more sets of doublets than previously noted by Promega (*22*) and six more than by Pattee (*23*). Currently, there is no explanation for these doublets. A size calibration was performed for this set of fragments on the basis of the published values, as shown in Figure 7. The important feature is the size separation within the sets of doublets rather than their absolute sizes or the percentage separation. This separation is not constant. So, size calibration indicates that they are not ligations of several bands due to the presence of small fragments. The extra bands would indicate an increase in the original chromosomal DNA size calculation from 3.1 to 3.5 Mb. These extra bands including a band at 500 bp were discovered due to the increased resolution in our separation. This shows the need for higher resolution for resolving bands throughout the separation. The separation performed here shows separation from 2.3 to 750 kb. A similar separation of *S. aureus* was performed with two constant pulse times, each of which took 15 h each to complete (*23*). The 6-s pulse only separated the lower size (48–242 kb), and the 20-s pulse only separated the higher series (242–700 kb). This research constitutes a decrease in separation time of at least 1 order of magnitude, even including the separation of fragments below 48 kb. Actually, the 560-bp fragment from *Hin*dIII is also completely separated from the others. The absorption signal there is much lower and the contrast was insufficient for visualization.

Other Considerations. The DNA fragment is left in its native state after separation, which means that specific site tagging and hybridization can proceed without further manipulation. The fact that no ethidium bromide, an intercalating dye which is mutagenic, or radioisotope labeling, which is a radiation hazard, is used to visualize the fragments has benefits because health risks are reduced. The DNA here can

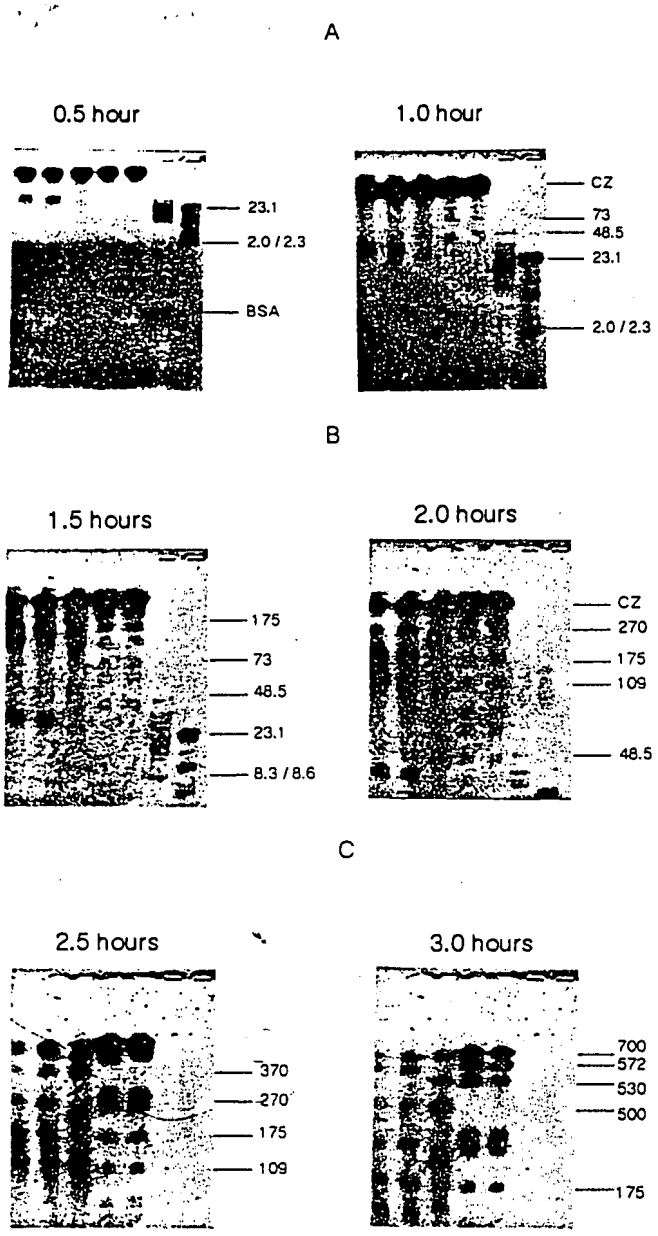

Figure 6. Images are from the three-hour separation utilizing the real time capabilities of the system to interactively control the pulse sequence. The pulse sequence is 0.6 s for 1 h, 3.0 s for 1 h, and 6.0 s for 1 h. Electrophoresis is from top to bottom in all images. Wells are at the top of the images. Note the HMW is not completely separated when the 3.0-s pulse is applied at 1 h but that sieving will further separate the fragments even when the pulse is not optimized to separate that fragment range. All the fragments in the two right lanes have moved off the gel by 2.5 h. Other conditions: 12 V/cm, 30 °C, 0.5% agarose, 10 mM TPE buffer, 16 frames averaged.

be isolated and further amplified by cloning or further fragmented (digested) or sequenced for higher resolution of its structure. Also, since tagging is not required, the migration rates are more reliable for estimating fragments sizes.

The 3-h separation was achieved by monitoring every $^1/_2$ h and deciding on the next pulse time. Obviously, if higher resolution were desired, the monitoring and decision intervals could be decreased. The 3-min data acquisition time is dictated by the lamp intensity and the present lamp and camera placement. A higher illumination intensity will shorten the exposure time without causing damage to the DNA. A closer placement of the camera will be even better, since the collection efficiency will increase.

These separations were performed on a 7-cm gel. This is considerably shorter than what most PFGE separations are usually run on. Obviously, the gel could hold many more

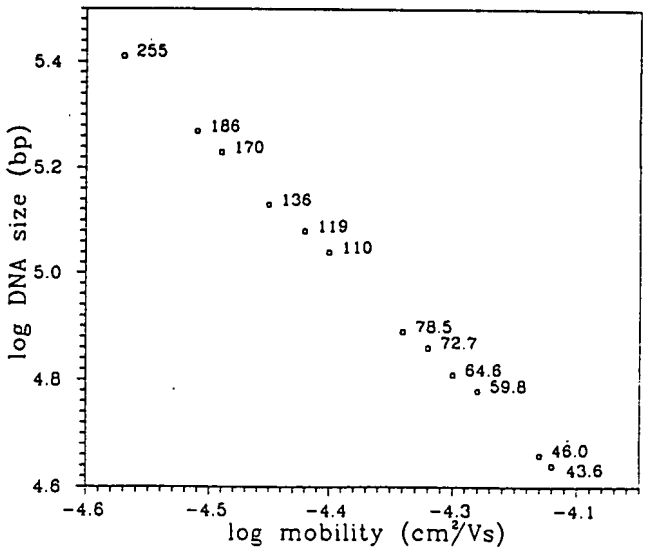

Figure 7. Graph of log DNA sizes vs log mobility of the doublets encountered in the separation of *S. aureus Csp* I. Note the differences ranging from 16 to 3.6 kb, indicating that ligation of fragments is not likely. Fragments at 255 and 136 kb are from another digest in the separation and are used strictly to extend the calibration. Other conditions: 12 V/cm, 30 °C, 0.5% agarose, 10 mM TPE buffer, 16 frames averaged.

fragments if the gel were twice as long. However, the size information is already contained in the early images for the smaller fragments. There was no need to retain those fragments on the gel. Short gels are advantageous because of the ease of casting, lower voltages required, and less dissipated power for the cooling system to handle. Extraction of the DNA from the gel could be accomplished by collecting at the edge of the gel in real time without affecting the separation in progress.

Quantitation of this detection scheme has been demonstrated previously by Chan et al. (*13*). Due to photon counting and two-dimensional ability of the CCD, it is possible to add up the entire absorbance of the band of DNA in question. It is then possible to accurately quantify the fragments in question. By this same capability, it would be possible to determine whether there is more than one band unresolved in the separation. When a certain amount of DNA is fragmented, smaller fragments will have a smaller mass and will have a linear dependence of integrated absorbance versus fragment size. Quantitation has not been pursued in this paper due to the nonquantitative nature of the supplied chromosomal samples. The current limit of detection for this system is around 2 ng of DNA, which is typical of PFGE studies. Detection limits for conventional forms of detection can be substantially lower, 10 pg to hundreds of picograms for ethidium bromide staining and femtograms to low picograms for radioisotope labeling. These detection limits are dependent on exposure times for their limits, which are 30-s to 30 min for ethidium bromide staining and hours to days exposure for radioisotope labeling. Exposure to photographic film also makes it difficult to quantitate over a large weight range. The quantities of DNA loaded on the gels in this experiment are typical amounts that are used in electrophoresis. DNA amounts should not be a problem because the ability to clone eliminates the need for working with very small amounts of DNA (*24*).

Rapid automated sequencing is becoming a reality. The ability to sequence in excess of 23 000 bp/h is feasible. However, further evaluation and automation are still needed in labor-intensive steps prior to sequencing. Our work shows that optimization and application of PFGE separations or ZIFE separations (*25*) can be speeded up substantially.

Naturally, there is still much time spent preparing and isolating the chromosomal DNA. This remains a major bottleneck on the way to mapping the entire human genome.

REFERENCES

(1) Andrew, L.; Olson, M. V. *Genetics* **1991**, *127*, 681–698.
(2) Jordan, E. *Anal. Chem.* **1991**, *63*, 420A–423A.
(3) Drossman, H.; Luckey, J. A.; Kostichka, A. J.; D'Cunha, J.; Smith, L. M. *Anal. Chem.* **1990**, *62*, 900–903.
(4) Schwartz, D. C.; Cantor, C. R. *Cell* **1984**, *37*, 67–75.
(5) Schwartz, D. C. In *New Directions in Electrophoretic Methods*; Jorgenson, J. W., Phillips, M., Eds.; ACS Symposium Series 335; American Chemical Society: Washington, DC, 1987; pp 167–181.
(6) Lal, E.; Birren, B. W.; Clark, S. M.; Simon, M. I.; Hood, L. *Biotechniques* **1989**, *7* (1), 34–42.
(7) Chu, G.; Vollrath, D.; Davis, R. W. *Science* **1986**, *234*, 1582–1585.
(8) Lalande, M.; Noolandi, J.; Turmel, C.; Rousseau, J.; Slater, G. W. *Proc. Natl. Acad. Sci. U.S.A.* **1987**, *84*, 8011–8015.
(9) Vlovy, J. L. *Biopolymers* **1987**, *26*, 1929–1940.
(10) Deutsch, J. M. *Science* **1988**, *240*, 922–924.
(11) Olson, M. V. *J. Chromatogr.* **1989**, *470*, 377–383.
(12) de la Cruz, M. O.; Gersappe, D.; Schaffer, E. O. *Phys. Rev. Lett.* **1990**, *64*, 2324–2327.
(13) Chan, K. C.; Koutny, L. B.; Yeung, E. S. *Anal. Chem.* **1991**, *63*, 746–750.
(14) Chu, G.; Vollrath, D.; Davis, R. Personal communication, Stanford University Medical Center, 1987.
(15) Dawkins, H. J. S. *J. Chromatogr.* **1989**, *492*, 615–639.
(16) Lewis, E. M.; Kourl, R. E.; Latorra, D.; Berka, K. M.; Lee, H. C.; Gaensslen, R. E. *J. Forensic Sci.* **1990**, *35*, 1186–1190.
(17) Fritsch, E. F.; Maniatis, T. *Molecular Cloning: A Laboratory Manual*, 2nd ed.; Cold Spring Harbor Laboratory Press: New York, 1989; p B.23.
(18) Woolley, P. *Electrophoresis* **1987**, *8*, 339–345.
(19) Noolandi, J.; Rousseau, J.; Slater, G. W.; Turmel, C.; Lalande, M. *Phys. Rev. Lett.* **1987**, *58*, 2428–2431.
(20) Ulanovsky, L.; Drouin, G.; Gilbert, W. *Nature* **1990**, *343*, 190–192.
(21) Pattee, P. A. *Genet. Maps* **1990**, *5*, 2.22–2.27.
(22) Hung, L. C.; Bandzkulis, R. *Promega Notes* **1990**, *24*, 1–3.
(23) Pattee, P. A. In *The Bacterial Chromosome*; Drlica, K., Riley, M., Eds.; John Wiley and Sons; New York, 1990; pp 163–169.
(24) Burke, D. T. *Genet. Anal.: Techn. Appl.* **1990**, *7* (5), 94–99.
(25) Noolandi, J. *Makromol. Chem., Rapid Commun.* **1991**, *12*, 31–35.

RECEIVED for review July 15, 1991. Accepted October 3, 1991. The Ames Laboratory is operated by Iowa State University for the U.S. Department of Energy under Contract W-7405-Eng-82. This work was supported by the Director of Energy Research, Office of Health and Environmental Research.

High-Performance

Jonathan V. Sweedler, Robert B. Bilhorn, Patrick M. Epperson, Gary R. Sims, and M. Bonner Denton
Department of Chemistry
University of Arizona
Tucson, Ariz. 85721

Numerous modern analytical techniques are based on detection and quantitation of light in the ultraviolet to near-IR regions of the spectrum. Sensitive atomic and molecular spectroscopies, including luminescence, absorption, emission, and Raman, require detectors with high responsivity, low read noise, large dynamic range, low dark count rate, and a linear or well-behaved response. Revolutionary developments in multichannel detectors have greatly expanded and improved the capabilities of current spectrochemical techniques.

INSTRUMENTATION

There is great interest in replacing single-channel photomultiplier tubes (PMTs) with multichannel devices (*1*, *2*). Multichannel detectors such as vidicons, intensified target vidicons, image dissectors, and photodiode arrays (PDAs) do not offer the sensitivity, dynamic range, and noise performance necessary to be competitive with the PMT in many situations. Successful application of these multichannel detectors is limited to experimental conditions in which the multichannel advantage outweighs the noise, cross talk, and dynamic-range disadvantages.

New multichannel alternatives to PMT detection are now capable of superior sensitivity and dynamic range when compared on a detector element by detector element basis. In fact, some of these devices exceed the sensitivity and dynamic range of all other available detectors. The performance of charge transfer devices (CTDs) has advanced to the point where the application of this technology to the field of analytical chemistry is appropriate. In the first of this two-part series, the theory, design, operation, and performance of CTD detectors are described. Part two, which focuses on a range of analytical applications, will appear in the March 1 issue of ANALYTICAL CHEMISTRY.

CTDs are solid-state multichannel detectors. These detectors integrate signal information as light strikes them, much like photographic film. An individual detector in a CTD array consists of several conductive electrodes overlying an insulating layer that forms a series of metal oxide semiconductor (MOS) capacitors. The insulator separates the electrodes from a doped silicon region used for photogenerated charge storage. The actual geometry of the electrodes and insulators varies, depending on the device and manufacturer.

The basic operation of a CTD detector element can be illustrated by considering the simple example shown in Figure 1, which depicts the cross section of a single-detector element made from *n*-doped silicon. In this *n*-doped silicon, the majority current carrier is the electron, and the minority carrier is the hole. When the electrodes are negatively charged with respect to the silicon, a charge inversion region is created under the electrodes. This region is an energetically favorable location for mobile holes to reside. The promotion of an electron into the semiconductor conduction band, such as by the absorption of a photon, creates a mobile hole that migrates to and is collected in the inversion region. In Figure 1, one electrode is held at a more negative potential than the other, making the accumulation of positive charge more favorable under this electrode.

The amount of charge generated in a CTD detector is measured either by

0003-2700/88/0360-282A/$01.50/0

Charge Transfer Device Detectors

moving the charge from the detector element where it is collected to a charge-sensing amplifier, or by moving it within the detector element and measuring the voltage change induced by this movement. These two modes of charge sensing are employed by the charge-coupled device (CCD) and the charge injection device (CID), respectively. Although CTDs made of *n*-doped silicon (commonly employed in CIDs) collect photogenerated holes, and CTDs made from *p*-doped silicon (commonly employed in CCDs) collect photogenerated electrons, by convention the photogenerated charge is always referred to in units of electrons. Complete descriptions of the operation of particular sensors appear in the optical engineering literature and can also be found in the chemical literature (see, e.g., References 1–7).

In the CCD, the charge from each detector element is shifted in sequence to an amplifier located at the end of a linear array or corner of a two-dimensional array of detector elements. Charge is transferred to the on-chip amplifier by sequentially passing the charge packets from one detector element to the next adjacent detector element. A series of electrodes in each detector element is used to perform this transfer. The number of independent electrodes used to effect this transfer ranges from one to four. Such CCDs appropriately are called uniphase to four-phase devices (*6*, *7*). The potentials of the electrodes in a detector element provide a barrier that separates adjacent charge packets. Shifting the location of this barrier in a controlled manner causes charge to migrate in the desired direction.

CCDs differ from other detectors by their ability to transfer the photogenerated signal from the photoactive element to an on-chip amplifier. This amplifier allows the CCD to obtain a very high signal-to-noise (S/N) output. Although digitization of the data in all CCD detector elements is not necessary, the architecture of the CCD requires shifting through the entire detector before proceeding to the next exposure; thus, subarrays may not be randomly read in CCD detectors.

The organization of a two-dimen-

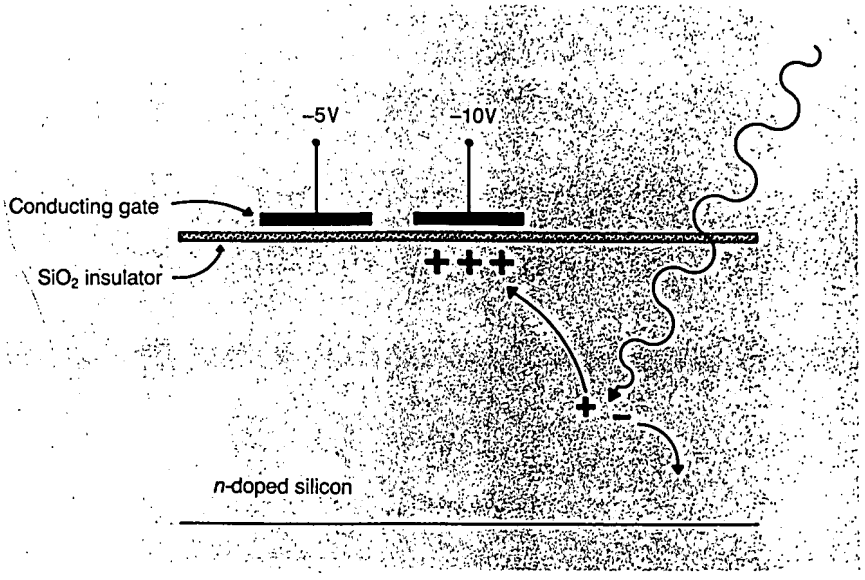

Figure 1. Cross section of a hypothetical CTD detector element when the electrodes are biased for charge integration.

The absorption of a photon causes hole–electron formation, and the positively charged hole is collected under the negatively charged electrode.

signal, three-phase CCD array is illustrated in Figure 2. Columns are clocked in parallel. With each clock, all of the charge in the imaging array is shifted toward the serial register by one row, whereas charge from the row adjacent to the serial register is transferred into the serial register. Once the charge is shifted into the serial register, the charge packets are shifted sequentially to the on-chip amplifier. The illumination of the CCD must be minimized during the charge transfer readout process to prevent blurring of the image. Fixed potential barriers between columns separate charge from adjacent columns. Extremely efficient transfer of charge from detector element to detector element is critical, because even small losses (~0.0001% loss per transfer) accumulate and become significant after the thousands of transfers required to read large CCDs. Modern CCDs are capable of thousands of charge transfers with almost immeasurable charge transfer losses (*8*, *9*).

A CID detector element consists of the intersection of two crossed electrodes. The electrodes are termed the *collection electrode* and the *sense electrode*. An array of collection and sense electrodes forms a network that allows individual detector elements to be addressed. Charge is kept in the detector element by potential barriers that prevent the photogenerated charge from migrating along the electrodes. Any individual CID detector element can be read by transferring the charge from under the collection electrode to the sense electrode and measuring the voltage change this induces on the sense electrode. Because this readout process does not alter the charge contained within the element, the process has been termed the *nondestructive readout mode* (*1*, *10*). Charge is cleared from a detector element by applying the substrate voltage to both electrodes, which injects the charge into the bulk silicon.

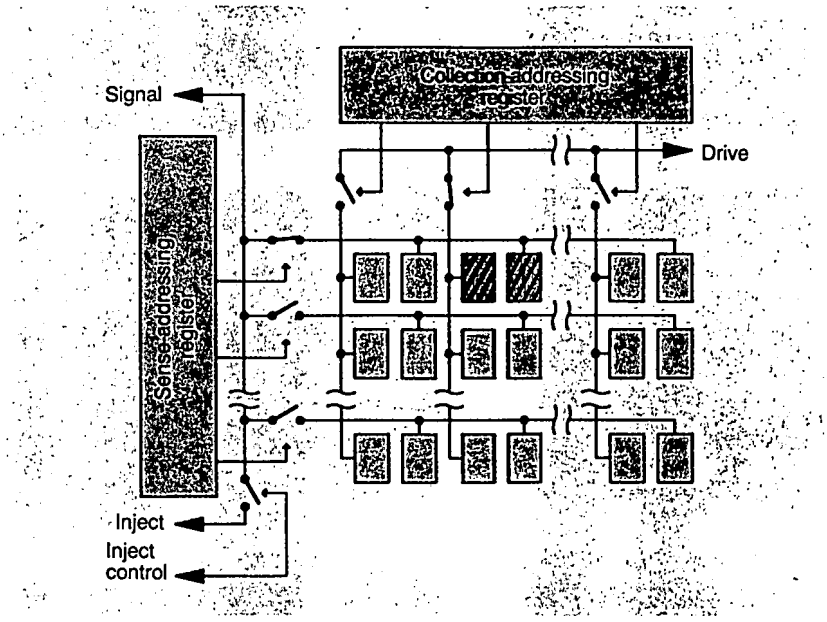

Figure 3. Hypothetical CID array detector showing the sense- and collection-addressing shift registers.

The registers open and close a series of switches to connect the collection and sense capacitor electrodes to the charge drive signal and output amplifier. The detector element at the intersection of the selected sense and collection capacitors is shaded (blue).

CIDs are fabricated to allow random access of any given detector element using high-speed shift registers for addressing. These registers connect the collection and sense electrodes to the drive signal and output amplifier, respectively, as shown in Figure 3. The integrated signal at the intersection of the selected collection and sense electrodes is either read using the nondestructive readout process or cleared using charge injection.

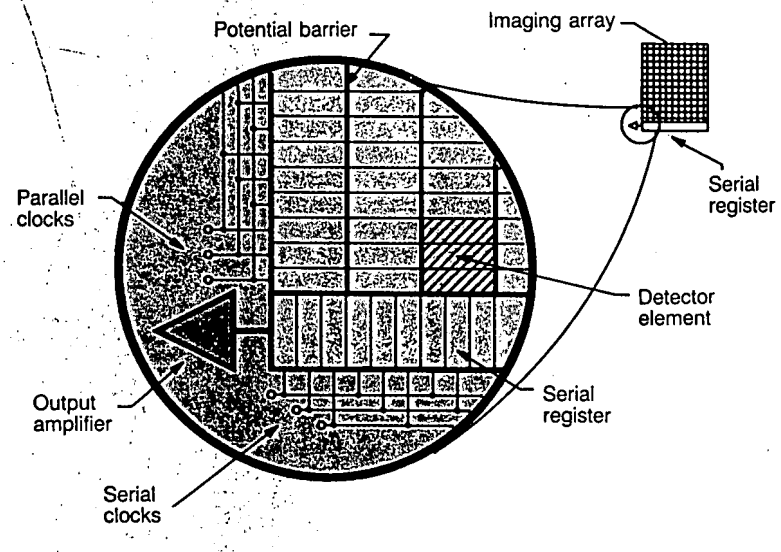

Figure 2. Layout of a typical three-phase CCD.

Photogenerated charge is shifted from the imaging area in parallel to the serial register (down in figure). The charge in the serial register is then shifted left to the on-chip amplifier and measured.

Format

The detector should not limit a spectroscopic system; rather, the ideal detector should be available in the correct physical format and size. Although not optimally configured for many current spectroscopic systems, CTDs are available with a wide variety of photoactive areas and number of detector elements. Figure 4 shows a collection of CTDs demonstrating their wide range of photoactive areas and formats.

Table I describes the characteristics of a variety of CTDs. The large number of detector elements available with some of the CTDs allows extremely high-resolution spectra to be obtained simultaneously. For example, an echelle spectrometer used in conjunction with a rectangular CTD containing several hundred thousand detector elements can cover the ultraviolet, visible, and near-IR spectral regions with > 0.01-nm resolution (*11*). Because of the large variety of available detectors, a CTD often can be selected for a specific application, matching the number of detector elements and device performance to experimental requirements. The relatively small size of the individual detector elements in most CTDs is a significant problem that requires ingenuity in optical design (*2*). The second article in this series will describe a variety of spectroscopic systems that effectively utilize these detectors.

Detector noise

A properly designed photon-counting PMT can detect individual photoelec-

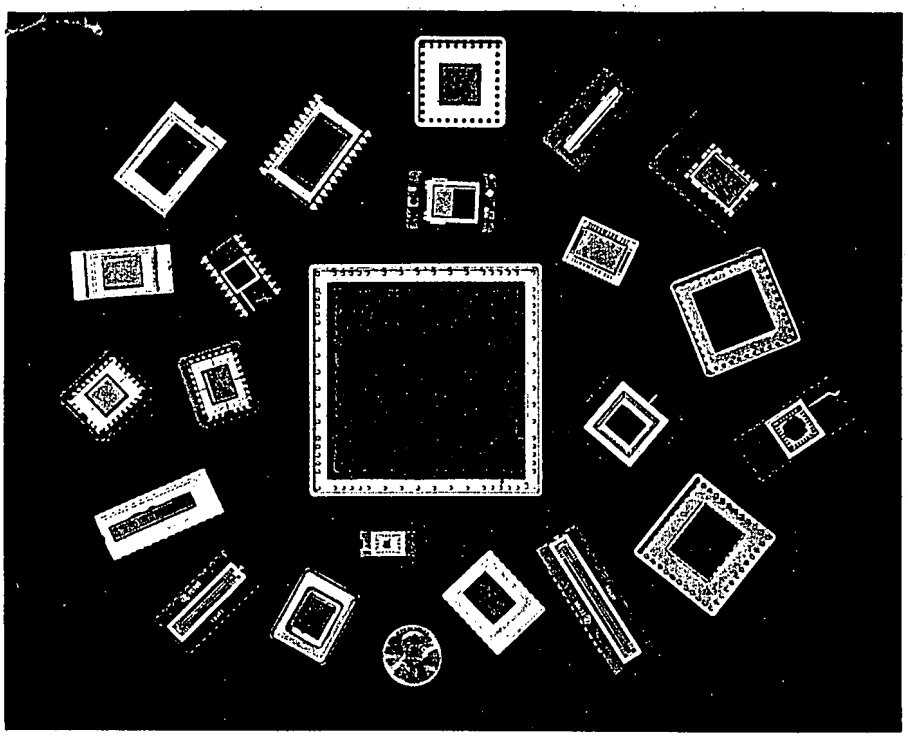

Figure 4. Photograph showing many of the charge transfer device detectors available during the past few years.

The number of detector elements ranges from 1 to more than 4 million, and the photoactive areas range from under 0.2 mm^2 to over 3000 mm^2. (Photograph courtesy of Photometrics Ltd., Tucson, Ariz.)

trons; that is, essentially no noise is associated with the actual readout of this detector. For integrating detectors, the situation is very different; integrating detectors such as CTDs and PDAs have a significant *read noise*—the noise introduced by the detector and associated electronics in reading out a single-charge packet. The magnitude of the read noise varies from more than 1200 electrons for scientific PDAs to fewer than 5 electrons for some low-noise CCDs. In CCDs, the sequential transfer of charge from the photosensitive area to a low-noise amplifier eliminates the multiplexing circuitry necessary in CIDs and PDAs, greatly reducing the capacitance on the amplifier input; therefore, the read noise is extremely low in these devices.

As previously mentioned, the CID detector can measure the charge information nondestructively. Nondestructively reading the CID multiple times and averaging the results decreases the effective read noise of the CID. This technique does not introduce any system or photon noise and hence increases the S/N ratio of a determination. To the extent that the read noise is white noise, the effective read noise is decreased as the square root of the number of averaged reads. In practice, the CID read noise is reduced by more than 1 order of magnitude by the process of averaging numerous nondestructive reads (*10*, *11*). The noise observed in current scientific CID systems approaches 1000 electrons but is reducible to fewer than 70 electrons using this method.

CCD detectors also have an imaginative readout mode called binning. *Binning* is the process of summing the charge contained in multiple elements on the detector before sensing the total charge (*12*). The charge in the binned group of detector elements is measured with a single read and hence has the noise associated with only one read. Binning can be contrasted to summation in computer memory, where the noise associated with reading each element contributes to the overall noise.

The advantage of summing the analog signal on chip using binning as opposed to digital summing in memory is illustrated in Figure 5, which shows the output of a CCD located at the focal plane of a molecular fluorescence in-

Table I. Characteristics of selected CTDs

Device	Architecture	Dimensions (elements)	Photoactive area (mm)	Peak QE (%) wavelength	Range over which QE exceeds 10%	Charge capacity (electrons)	Read noise (electrons)
General Electric CID17-B	CID	244 × 388	6.5 × 8.7	47% at 500 nm	210–850 nm	6×10^5	60
General Electric CID751	CID	1 × 1	1.0 × 1.0	35% at 250 nm	200[a]–850 nm	1×10^8	80
Kodak M1A	Frontside CCD	1035 × 1320	7.0 × 9.0	37% at 700 nm	450–900 nm	1.4×10^5	10
Reticon	Frontside CCD	404 × 128	21.0 × 6.6	NA	420–1000 nm	2×10^6	45
RCA SID501EX[b]	Backside CCD	512 × 320	15.4 × 9.6	90% at 500 nm	200[a]–950 nm	4×10^5	750
Tektronix TK512M-0-1	Frontside CCD	512 × 512	13.8 × 13.8	35% at 750 nm	450–950 nm	9×10^5	46
Texas Instruments	Backside CCD	800 × 800	12.0 × 12.0	90% at 550 nm	0.1[a]–1000 nm	5×10^4	7
Texas Instruments TC104-1	Frontside CCD	3456 × 1	35.6 × 0.1	90% at 400 nm	200[a]–950 nm	3×10^5	80
Thomson-CSF TH7882CDA	Frontside CCD	384 × 576	8.8 × 13.2	45% at 650 nm	420–950 nm	5×10^5	10

[a] Point at which quantum efficiency (QE) measurements stopped. QE may exceed 10% beyond this point. [b] Detectors received additional processing.

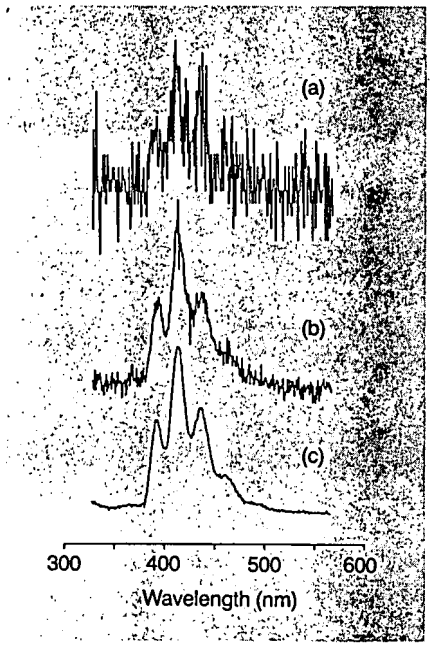

Figure 5. Fluorescence spectra of anthracene obtained with a CCD detector.

The slit image illuminates 64 rows of the CCD. Results are shown for three methods of reading out the CCD with each spectrum scaled for comparison. (a) The anthracene spectrum obtained from reading only one of the 64 illuminated rows of the CCD. (b) The result of reading out and summing in computer memory all 64 rows of the slit image. The resulting spectrum has ~ 8 times the S/N ratio of the spectrum in (a). (c) The output of the CCD when the photogenerated charge from all 64 rows is binned into a single row and the single binned row is read. The spectrum in (c), which has the same absolute signal as in (b), has ~ 64 times the S/N ratio of the spectrum in (a).

strument (*13*). The vertical image of the slit corresponds to 64 rows of the CCD, whereas the wavelength is displayed in the horizontal dimension. Binning in the slit direction increases the S/N ratio of the spectrum compared with summing in computer memory. Binning in the wavelength direction also increases the S/N ratio of the spectra, albeit at a loss of resolution (*4*).

For low-light-level spectroscopy, when the dominant source of noise is detector read noise, computer memory summation is noisier by a factor equal to the square root of the number of summed elements as compared with on-detector binning. Figure 5 shows anthracene spectra measured by reading a single row of the spectrum, reading out all 64 rows and summing in computer memory, and reading the charge information by binning the 64 rows together and reading out this single binned row. As can be seen, the binned mode results in a much higher S/N ratio spectrum.

For low-light-level spectroscopy, the dark current, or thermal generation of signal, is an important detector parameter directly affecting the maximum observation time. For silicon array detectors, the majority of the thermally generated charge appears at defects in the bulk silicon and at the surface silicon–silicon oxide interface; subsequently, dark current is dependent on the manufacturing process and geometry. CCDs used in low-light-level applications are cooled between −30 °C and −150 °C, so that the dark current is extremely low. However, CCDs cannot be cooled to arbitrarily low temperatures to further reduce the dark current. The ability to transfer the photogenerated charge decreases as the temperature is reduced, giving an absolute temperature limit of operation for most CCDs of approximately −150 °C. In a CID, the charge is transferred between electrodes in a single-detector element. Thus they can be operated at lower temperatures because the small amount of charge left behind in one transfer is subsequently collected in the next transfer. Therefore charge losses are not accumulative as in CCDs. The dark current for most properly cooled CCDs is in the range of 0.03 to < 0.001 e^-/s, and for CIDs the dark current is < 0.008 e^-/s. Dark currents of these levels are insignificant for most analytical spectroscopic applications. Exposures of minutes are required before the dark current is even measurable, and theoretically, exposures of years are required before the devices saturate.

Spectral responsivity

In many situations the most important characteristic of an optical radiation detector influencing the S/N ratio of a measurement is the detector quantum efficiency. The intrinsic quantum efficiency of all silicon detectors (PDAs, CTDs, etc.) is high compared with the quantum efficiency of available photoemissive materials in the visible to near-IR wavelength region. The measured quantum efficiency of silicon detectors varies greatly, depending on the structure of the detector (see Table I). Figure 6 shows the quantum efficiency of representative detectors in the 200–1000-nm wavelength region.

In addition to having a high quantum efficiency in the ultraviolet to the near-IR regions, some CTDs can directly measure photons in the vacuum ultraviolet and the soft X-ray regions (*9*, *14–15*). The quantum efficiency for these high-energy photons depends greatly on the structure of the detector and the thickness of the overlying oxide. Quantum efficiencies exceeding 50% have been reported. In addition to X-ray imaging applications, these CTDs can also be used as direct energy-dispersive imaging detectors because the measured signal is proportional to the energy of the X-ray photon. One hole–electron pair is created for every 3.65 eV of photon energy. For example, Mn Kα (5.9 KeV) photons produce 1620 e^-. The energy resolution of the detector depends on the system read noise as well as the ability of the detector to contain all the charge information accurately (i.e., the charge created by a single X-ray event should not be split among neighboring detector elements). For low-noise CCDs, the energy resolution obtainable is 150 eV for photon energies > 1000 eV. Figure 7 shows an X-ray spectrum obtained using a ^{55}Fe source.

The bandgap of silicon limits the response to photons with wavelengths shorter than ≈1200 nm. Considerable

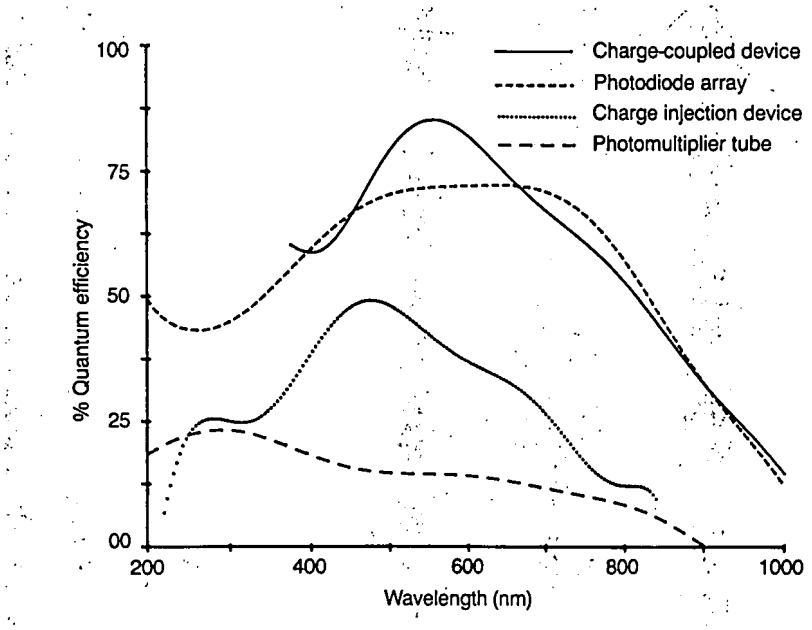

Figure 6. Quantum efficiency of several representative detectors: a Texas Instruments 800 × 800 CCD (*9*), a General Electric 244 × 388 CID, a Reticon RL1024S PDA, and a Hammamatsu GaAs opaque photocathode available in PMTs.

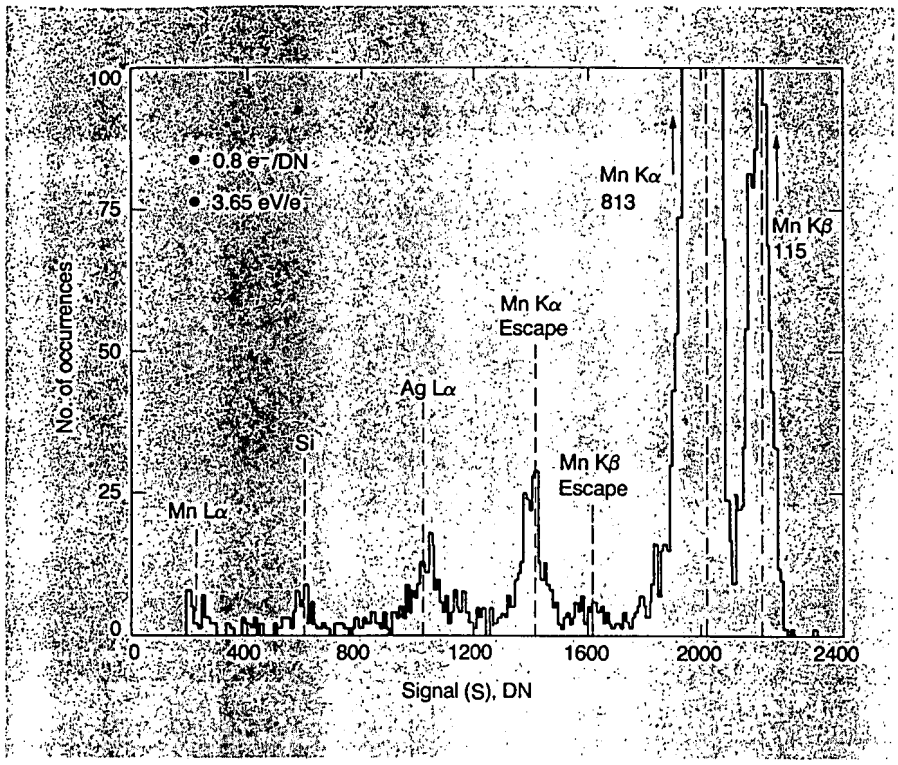

Figure 7. X-ray spectrum of a ^{55}Fe X-ray source using a CCD as an energy-dispersive detector showing the Mn Kα and Mn Kβ lines, as well as both escape peaks and the silicon absorption peak.

The Ag Lα peak is from Ag impurity in the source. The peak energy is obtained by multiplying the signal by a factor combining the CCD gain of 0.8 e^- per digital number (DN) and the 3.65 eV of photon energy per electron produced (2.92 eV/DN). (Adapted with permission from Reference 9.)

effort has been devoted to extending the longer wavelength range of CTD detectors by making them out of a variety of materials, including germanium, indium antimonide, and platinum silicide (*7*, *16*). The performance of these nonsilicon CTDs is expected to improve rapidly. Near- and mid-IR spectroscopy should greatly benefit with the advent of high-quality, low-noise multichannel detectors that respond in these regions.

Spectroscopic characteristics

Low-light-level spectroscopies such as Raman and luminescence place stringent demands on a detector system. High responsivity, minimal read noise, and negligible dark current are all necessary for low-flux conditions. Figure 8 shows the calculated S/N ratio for the Texas Instruments 800 × 800 CCD and the GE 244 × 388 CID listed in Table I, as well as a representative photomultiplier tube and photodiode array under low-flux conditions. In addition, the S/N ratio for the perfect photon detector is shown, with an assumed 100% quantum efficiency (QE), zero read noise, and no dark current. The only noise source in this curve is the photon shot noise. The comparison shown is for a 10 photons-per-second illumination level at a wavelength of 600 nm with observation times of 0–100 s.

For the real detectors, these calculations include the effects of photon shot noise, photon flux, detector QE, read noise, and dark current shot noise (*1*). The comparisons are made on a detector element by detector element basis and do not include any multichannel advantages. The photon-counting photomultiplier tube used in this comparison has a dark count rate of 5 counts per second, and the photodiode array has a dark count rate of 3×10^4 e^-/s at −20 °C and a read noise of 1200 e^-. Whereas almost all commercial PDA systems allow cooling to −20 °C, the dark current of the PDA can be reduced significantly by further cooling.

As shown in Figure 8, the CCD has the highest S/N ratio of any of the listed detectors and is only 11% lower than that of the perfect photon detector after 100 s. The sensitivity of CCDs has long been exploited by astronomers (*17–19*) and is beginning to be recognized by researchers in other fields (*13*, *20–22*).

The ability of a detector to measure photon fluxes that vary over a wide range is important in spectroscopic applications. The range of photon fluxes that the detector can quantify depends on a number of parameters, both detector related (such as maximum readout rate, maximum integration time, read noise, and dark current) and system dependent (such as the number and relative intensities of the spectral features, maximum observation time, and source drift). These detectors have a *simple dynamic range* defined as the ratio of the maximum amount of charge that can be contained in a detector element to the minimum amount of charge that can be measured. The simple dynamic range of some modern CCDs approaches 1 million—large enough for many spectroscopic applications.

In some areas of spectroscopy, the

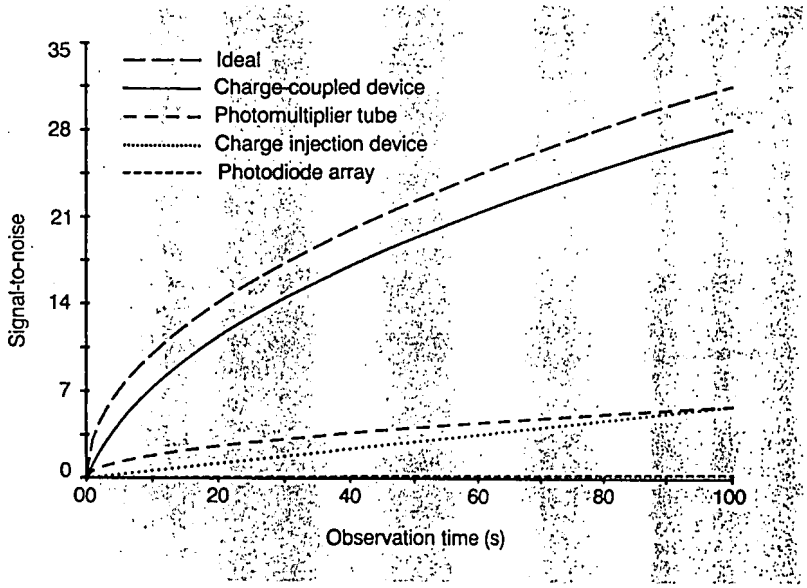

Figure 8. Calculated performance curves for the same detectors as in Figure 6 showing the S/N ratio obtained for a single detector element with a photon flux of 10 photons/s for observation times ranging from 0 to 100 s at a wavelength of 600 nm.

The top curve is for the perfect photon detector with 100% quantum efficiency and no noise sources except photon shot noise (the uncertainty caused by the random arrival of photons to the detector). The model used in these calculations includes the effects of photon shot noise, detector read noise, detector quantum efficiency, and detector dark current. (See text for other detector characteristics.)

ability to measure faint spectral lines in the presence of bright spectral features is important. The intense features should not influence the quantitation of the weak features. Some CTDs can suffer from problems when the charge storage ability of a detector element is exceeded. After the charge capacity of an individual CTD detector is reached, additional charge can spill into nearby detector elements in a process called *blooming*. Charge that blooms from a detector element exposed to a high photon flux can mask the signal of nearby elements. There are several methods used to alleviate blooming in CTDs. In CIDs, the excess charge is transferred into the substrate. In addition, some CCDs are fabricated with antiblooming structures.

CIDs allow a means of extending their effective dynamic range using a process called *random access integration*, in which the actual integration times are varied during a given experiment from detector element to element based on the amount of light reaching each element. In practice, this is achieved by scanning through the device, reading each detector element nondestructively, and determining the signal level at each element. A decision determining optimum integration time is based on the observed photon flux. Quantitation is achieved by storing the observed signal and integration time. Using this method, strong lines are integrated for short periods, and weak features are allowed to integrate until sufficient S/N ratio is obtained. In atomic emission spectroscopy, dynamic ranges exceeding 7 orders of magnitude have been quantified using the random access integration time technique with CID detection (*11*).

Conclusions

CIDs and CCDs have great potential to solve challenging spectroscopic problems. CTDs offer negligible dark currents, peak quantum efficiencies of more than 80%, low read noises, and wide dynamic ranges. In addition, the ability of CCDs to bin photogenerated charge from multiple elements and the nondestructive readout mode of CIDs contribute to the flexibility these detectors offer to the spectroscopist. These detectors are available from several manufacturers in a variety of formats and sizes that respond over a wide wavelength range. Although the application of this technology to analytical spectroscopy has been slow, CTDs are currently being used with impressive results. The second article in this series will describe the use of CTD detectors to overcome a variety of difficult analytical problems. Future applications of CTDs will continue to broaden the utility and increase the performance of many areas of spectroscopy.

The authors thank James R. Janesick of Jet Propulsion Laboratory for use of the ^{55}Fe X-ray spectrum, Richard Aikens of Photometrics Ltd., and Phillip Miller of Lawrence Livermore National Laboratory. This article is based on work partially funded by the Office of Naval Research and by SmithKline Beckman.

References

(1) Bilhorn, R. B.; Sweedler, J. V.; Epperson, P. M.; Denton, M. B. *Appl. Spectrosc.* **1987**, *41*(7), 1114.
(2) Bilhorn, R. B.; Epperson P. M.; Sweedler J. V.; Denton M. B. *Appl. Spectrosc.* **1987**, *41*(7), 1125.
(3) Sims, G. R.; Denton, M. B. In *Multichannel Image Detectors*; Talmi, Y., Ed.; ACS Symposium Series 236; American Chemical Society: Washington, D.C., 1983; Vol. 2, Chap. 5.
(4) Denton, M. B.; Lewis, H. A.; Sims, G. R. In *Multichannel Image Detectors*: Talmi, Y., Ed.; ACS Symposium Series 236, American Chemical Society: Washington, D.C., 1983; Vol 2., Chap. 6.
(5) See *J. Opt. Eng.* **1987**, *26* (8, 9, 10).
(6) Janesick, J. R.; Elliott, T.; Collins, S.; Marsh, H.; Blouke, M.; Freeman J. *Proc. SPIE* **1984**, *501*, 2.
(7) Dereniak, E. L.; Crowe, D. G. *Optical Radiation Detectors*; John Wiley: New York, 1984.
(8) Epperson, P. M.; Sweedler, J. V.; Denton, M. B.; Sims, G. R.; McCurnin, T. W.; Aikens, R. S. *J. Opt. Eng.* **1987**, *26*, 715.
(9) Janesick, J. R.; Elliot, T.; Collins, S.; Blouke, M. M.; Freeman, J. "Scientific Charge-Coupled Devices"; *J. Opt. Eng.* **1987**, *26*, 692.
(10) Sims, G. R; Denton, M. B. *J. Opt. Eng.* **1987**, *26*, 1008.
(11) Bilhorn, R. B. Ph.D. Dissertation, University of Arizona, 1987.
(12) Epperson, P. M.; Denton, M. B., submitted for publication in *Anal. Chem.*
(13) Epperson, P. M.; Jalkian, R. A.; Denton, M. B., unpublished results.
(14) Stern, R. A.; Liewer, K.; Janesick, J. R. *Rev. Sci. Instrum.* **1983**, *54*, 198.
(15) Janesick, J. R.; Campbell, D.; Elliott, T.; Daud, T.; Ottley, P. *Proc. SPIE* **1986**, *687*, 36.
(16) See *J. Opt. Eng.* **1987**, *26*(3).
(17) Oke, J. B. *Proc. SPIE* **1981**, *290*, 45.
(18) Goad, L. E. *Proc. SPIE* **1982**, *331*, 130.
(19) York, D. G.; Jenkins, E. B.; Zucchino, P.; Lowrance, J. L.; Long, D.: Songaila, A. *Proc. SPIE* **1981**, *290*, 202.
(20) Murray, C. A.; Dierker, S. B. *J. Opt. Soc. Am. A* **1986**, *3*, 2151.
(21) Strauss, M. G.; Naday, I.; Sherman, I. S.; Zaluzec, N.J. *Ultramicroscopy* **1987**, *22*, 117.
(22) Hiraoka, Y.; Sedat, J.W.; Agard, D.A. *Science* **1987**, *238*, 36.

M. Bonner Denton (top left) is a professor of analytical chemistry at the University of Arizona. He received a B.S. in chemistry and a B.A. in psychology from Lamar University (Beaumont, Tex.) and a Ph.D. in chemistry from the University of Illinois, Champaign–Urbana, where he studied under Howard Malmstadt. His research interests include the application of the latest technological advances in electronics, physics, optics, astronomy, acoustics, mechanical engineering, and computer science to the development of new and improved methods of chemical analysis and automation.

Patrick M. Epperson (top right) is a scientist at the Lawrence Livermore National Laboratory (Livermore, Calif.). He received his B.A. in chemistry from Occidental College, Los Angeles, in 1981, and his Ph.D. in analytical chemistry from the University of Arizona in 1987. His research interests include the application of charge-coupled device detectors for low-light-level spectroscopy and the design of spectrographs using two-dimensional array detectors.

Robert B. Bilhorn (bottom left) is a research chemist in the Analytical Technology Division of Eastman Kodak (Rochester, N.Y.). He received his B.S. in chemistry from the University of Florida at Gainesville (1981) and his Ph.D. in analytical chemistry from the University of Arizona (1987). His research interests are developing expert systems and applying charge transfer device detectors to challenging analytical problems.

Jonathan V. Sweedler (bottom right) is pursuing his Ph.D. in analytical chemistry at the University of Arizona. He received his B.S. in chemistry from the University of California at Davis in 1983. During the summers of 1980 through 1982 he worked at Lawrence Livermore National Laboratory, and he has also been a consultant for Photometrics Ltd. His research interests include the application of charge transfer device detectors to analytical spectroscopy and the use of novel holographic spectroscopic techniques in atomic and molecular spectroscopy.

Gary R. Sims is the manager of research and applications at Photometrics Ltd. (Tucson, Ariz.). He received a B.S. degree in chemistry from the University of Missouri, Columbia (1979) and a Ph.D. in analytical chemistry from the University of Arizona (1988). His research interests include the application of advanced solid-state imaging detectors for multichannel spectroscopic chemical analysis.